EFFECT OF SAMARIUM SUBSTITUTION WITH BISMUTH ON TRANSPORT AND MAGNETORESISTANCE PROPERTIES OF Bi-2223

by

SERDAR ŞAHİN

THESIS SUBMITTED TO
THE GRADUATE SCHOOL OF NATURAL AND APPLIED SCIENCES
OF
THE ABANT İZZET BAYSAL UNIVERSITY
IN PARTIAL FULFILLMENT OF THE REQUIREMENTS FOR THE
DEGREE OF MASTER OF SCIENCE
IN
THE DEPARTMENT OF PHYSICS

NOVEMBER 2013

Approval of the Graduate School of Natural and Applied Science

Prof. Dr. Yaşar DÜRÜST
Director

I certify that this thesis satisfies all the requirements as a thesis for the degree of Master of Science.

Prof. Dr. İbrahim Belenli
Head of Physics Department

This is to certify that we have read this thesis and that in our opinion it is fully adequate, in scope and quality as a thesis for the degree of Master of Science.

Asist. Prof. Dr. Gürcan YILDIRIM
Co-Supervisor

Prof. Dr. Cabir TERZİOĞLU
Supervisor

Examining Committee Members:

1. Prof. Dr. Cabir TERZİOĞLU...
2. Assoc. Prof. Dr. Osman GÖRÜR..
3. Assoc. Prof. Dr. Özgür ÖZTÜRK...
4. Asist. Prof. Dr. Gürcan YILDIRIM ....
5. Asist. Prof. Dr. Muhammet YILDIRIM ....

ABSTRACT

EFFECT OF SAMARIUM SUBSTITUTION WITH BISMUTH ON TRANSPORT AND MAGNETORESISTANCE PROPERTIES OF Bi-2223

ŞAHİN, Serdar

Master of Science, Department of Physics

Advisor: Prof. Dr. Cabir TERZİOĞLU

November 2013, 56 Pages

The aim of this study is to examine the effects of Sm subsititution with Bi on the structural and superconducting properties of Bi-2223 ceramics with the aid of the DC electrical resistivity, critical current density, XRD and SEM measurements. One of the most important progresses has been achieved in enhancing the transport properties of this high-Tc superconductor with DC electrical resistivity since the discovery of Bi-2223 superconductor. Besides the measurements of XRD are used to understand both lattice parameters and phase composition. The images of scanning electron microscopy (SEM) are used for microstructure examination. The substitution of Sm with Bi on Bi-2223 is performed with changing the concentration of Sm as x = 0, 0.01, 0.03, 0.05 0.07, 0.1 and 0.3. The superconducting samples were synthesized by the solid state reaction method to obtain information about the growth techniques. Solid state reaction method is the conventional method to prepare superconductors. The critical temperature was increased until the concentration of Sm x=0.3.

The samples studied in this study are prepared by conventional solid-state reaction method at the annealing temperature of 840°C for 48h. For the potential technological and industrial applications, the important characteristics such as the normal state resistivity, density, porosity, critical (onset and offset) transition temperature, variation of critical temperature, self field critical current density, crystallinity, phase purity, lattice parameter, texturing, surface morphology, Vickers microhardness and elastic modulus values are obtained for the pure and Sm substituted samples and compared with each other. At the same time, the Vickers microhardness values indicate that the samples (towards optimally doped state) exhibit Reverse Indentation Size Effect (RISE) behavior.

As for SEM images, similar to the XRD investigations, the former sample has the best crystallinity, texturing, grain connectivity, lowest porosity and largest grain size while the worst surface morphology is observed for the latter sample. Additionally, the bulk porosity analyses for the samples demonstrate that the bulk porosity decreases monotonously with the Sm content in the Bi-2223 system up to x=0.1 after which the porosity starts to increase regularly towards to maximum value, leading to the degradation of the grain connectivity.

Keywords: XRD, SEM, Bi-2223, T_c; J_c; $H_{v,}$ Vickers

ÖZET

SAMARYUMUN İLE BİZMUT YER DEĞİŞİMİNİN Bi-2223 SÜPERİLETKEN SERAMİKLERİNİN TRANSPORT VE MAGNETORESİSTANS ÖZELLİKLERİ ÜZERİNE ETKİSİ

ŞAHİN, Serdar

Yüksek Lisans, Fizik Bölümü

Tez Danışman: Prof. Dr. Cabir TERZİOĞLU

Kasım 2013, 56 Sayfa

Bu çalışmanın amacı DC elektriksel özdirenç, kritik akım yoğunluğu, XRD ve SEM ölçümler yardımıyla Bi ile Sm'un yer değiştirmesinin etkilerini, Bi-2223 seramiklerinin süperiletken ve yapısal özellikleri üzerinde incelemektir. Bi-2223 süperiletken keşfinden bu yana en önemli gelişmelerden birine DC elektrik direnç ile bu yüksek Tc süperiletken iletim özelliklerinin artmasıyla ulaşılmıştır. Bunun yanı sıra XRD ölçümleri hem lattice parametreleri hem de faz bileşimi anlamak için kullanılır. Elektron mikroskobu tarama görüntüleri (SEM) mikroyapı incelemeleri için kullanıldı. Bi-2223 üzerinde Bi ile Sm'un yer değiştirmesi, Sm'un konsantrasyonunun x = 0, 0.01, 0.03, 0.05, 0.07, 0.1 ve 0.3 olarak değiştirilmesiyle gerçekleştirilmiştir. Süperiletken örnekleri, gelişmiş teknikler hakkında bilgi elde etmek için katı hal reaksiyonu metodu ile sentezlenmiştir. Katı hal reaksiyonu yöntemi süperiletken

hazırlamak için geleneksel bir yöntemdir. Samaryumun kritik sıcaklığı Tc; samaryum konsantrasyonu x = 0.3 olana kadar artmıştır.

Bu çalışmada kullanılan 840°C tavlama sıcaklığında örnekler bilinen katı hal reaksiyon yöntemiyle hazırlanmıştır. Normal durum direnç, yoğunluk, gözeneklilik, kritik sıcaklık kritik (başlangıç ve ofset) geçiş sıcaklığı, kritik sıcaklıktaki değişim, kendini alanında kritik akım yoğunluğu, kristal, faz saflık, kafes parametresi, doku, yüzey morfolojisi, Vickers sertlik ve elastik modülü gibi potansiyel teknolojik ve endüstriyel uygulamalar için önemli olan ölçümler saf ve Sm eklenmiş ölçümler için alınmış ve birbirleri ile karşılaştırılmıştır. Aynı zamanda, Vickers sertlik değerleri örnekleri (optimum katkılı yapıya doğru) Ters Girinti Boyut Etkisi (TGBE) davranışı göstermektedir.

XRD datalarına benzer olarak SEM ölçümleri de ilk örneğin en iyi kristal, doku, tane bağlantı, düşük gözeneklilik ve en büyük tane boyutu özelliklerine sahipken sonraki örneklerde yüzey yapısının bozulduğunu görmekteyiz. Buna ek olarak, örnekler için hacim-gözeneklilik analizinin sonucu olarak Bi-2223 yapısındaki gözenekliliğin x=1'e kadar Sm miktarı ile monoton bir biçimde düştüğünü görmekteyiz. Doku, tane bağlantı kısımlarının bozulmasından dolayı da belirtilen x miktarının üstünde gözeneklilik maksimum olana kadar artmaktadır.

Anahtar Kelimeler: XRD, SEM, Bi-2223, T_c; J_c; H_v, Vickers

To My Favorite Team "Trabzonspor"

ACKNOWLEDGMENTS

I would like to thank My Supervisor, Prof. Dr. Cabir TERZİOĞLU for his guidance and support throughout this thesis and also with my professional development.

Special thanks are given to Assist. Prof. Dr. Gürcan YILDIRIM, being always accessible, and willing to help throughout this dissertation. I would like to thank my thesis committee members for their guidance and assistance through this process. Of course, their discussion, comments, ideas and especially feedback have certainly been invaluable to interpret and improve the results obtained.

I would like to thank also jury members, Assoc. Prof. Dr. Osman GÖRÜR., Assist. Prof. Dr. Muhammet YILDIRIM for their cooperation and suggestions for this study and Assoc. Prof. Dr. Özgür ÖZTÜRK, who is a lecturer in the department of physics of Kastamonu University, for helping me to investigate the microhardness measurements about my master thesis.

I would also like to thank my research friend Şenol KAYA, who is an expert of effects of radiation on electrical characteristics of BFO MOS capacitor, Uğur SOYKAN, Fırat KARABOĞA, Musa DOĞRUER who act as brothers throughout my thesis and also RA Asaf Tolga ÜLGEN for their supports, and help during my research.

I am very grateful to my amazing parents: Grandpa, Dad, Mom and Sister for their love, moral support, constant encouragement, and prayers throughout this process.

TABLE OF CONTENTS

LIST OF TABLES

LIST OF FIGURES

CHAPTER 1

INTRODUCTION

As known, motion of negative and positive charges in material creates electrical current. Drift motion of electron under applied electric field caused electrical current in metal surface.

The application of a voltage is necessary to pass a current through conductive material is defination of resistor. The result of the current flowing through the conductor has been heating at the material. The greater the resistance is, the greater the voltage to be applied, and the lost energy is. However, some conductor materials, the so-called critical temperature cooled to a temperature below the current-carrying electrons lose the converting capabilities from their energy to heat and the resistance drops to zero. In this case, a voltage application and energy without losing any current it becomes possible to create and the material is cooled below the critical temperature, the phonon effect is eliminated and electrons can easily move within the structure as without any interactions with lattice. The resistance of the structure below the critical temperature suddenly drops to zero. Below the critical temperature of the material, this material is called superconducting.

Superconductors, materials that have no resistance to the flow of electricity, are one of the last great frontiers of scientific discovery. Not only have the limits of superconductivity not yet been reached, but also the theories that explain superconductor behavior seem to be constantly under review. In 1911 superconductivity was first observed in mercury by Dutch physicist Heike Kamerlingh Onnes in Leiden University. Onnes was able to measure the electrical resistance of metals at low temperature. The startling discovery made in 1911 was that as the temperature of a sample of Hg was reduced, the resistance did not fall continuously as expected, but instead at around 4.2 K dropped suddenly to zero over a range of a few hundredths of a degree. In other words, when he cooled it to the temperature of liquid helium, 4^{o}Kelvin (-452F, -269C), its resistance suddenly disappeared. The Kelvin scale represents an "absolute" scale of temperature. Thus, it was necessary to come within 4 degrees of the coldest temperature that is theoretically attainable to witness the phenomenon of superconductivity [1].

In 1911, Onnes began to investigate the electrical properties of metals in extremely cold temperatures. It had been known for many years that the resistance of metals fell when cooled below room temperature, but it was not known what limiting value the resistance would approach, if the temperature were reduced to very close to 0 K. Some scientists, such as William Kelvin, believed that electrons flowing through a conductor would come to a complete halt as the temperature approached absolute zero.

Another important property of superconductors was discovered by Meissener & Ochsenfeld in 1933. One would expect, due to the perfect conductivity, that magnetic flux should be excluded from entering a superconductor, but also it was found that flux was expelled from the material as it was cooled through its trasition temperature. This phenomenon is termed the Meissener Effect. The expulsion of the magnetic field requires the flow of circulating 'screening current' and hence the existence of the Meissener effect necessitates that the resistance must be zero. This ‘perfect diamagnetisim’ demostrates that the superconductivity is a true thermodynamics state and that in moving from the normal to the superconducting state, a material undergoes a thermodynamic phase transition. In order to ensure this, the overall free energy must be lower in the superconducting state than in the normal state and this energy difference is related to the temperature.

Since the discovery of the copper oxide based superconductors; numerous investigations have been carried out to characterize properties of bismuth superconducting materials. In recent researches on superconducting ceramics, the Bi–Sr–Ca–Cu–O (BSCCO) superconducting compound has received much attention because of its high critical temperature, Tc, and its high critical current density, Jc. It has been known that chemical doping plays a very important role in high-Tc superconductivity. Several studies of doping into superconductor oxide ceramics have been performed in order to enhance their physical and mechanical characteristics [2-4]. Experimentally, the superconducting transition temperature Tc becomes higher with an increasing number of CuO_2 layers. The high Tc (Bi, Pb)SrCaCu-2:2:2:3 (110 K) phase is extremely difficult to prepare in a pure form since it usually intergrows with the BiSrCaCu-2:2:1:2 (85 K) phase. The objectives of doping works are to optimize the hole concentration, to introduce pinning centers, and to enhance the formation of Bi-2223 phase [5].

The effects of substitution of Sm with Bi in Bi-2223 superconductor on microstructure, superconducting and mechanical properties was investigated that superconducting properties (the values of Tc and Jc) and mechanical properties (microhardness) degrade with increasing Sm content.

CHAPTER 2

THE PROPORTIES OF SUPERCONDUCTIVITY

2.1 The Historical Development of superconductivity

Superconductivity begins with Kammerlingh Onnes' [6] discovery that electrical resistance of mercury suddenly vanished near the absolute zero of temperature, namely close to 4 K. It was thought for sometimes that superconductivity was a state of perfect frictionless flow of electricity and that the resistanceless state of superconductors was the fundamental property [7]. The next great milestone in understanding how matter behaves at extreme cold temperatures was in 1933. Walter Meissner and Robert Ochsenfeld [8] discovered that a superconductor repels a magnetic field. A magnet moving by a conductor induces currents in the conductor. This is the principle upon which the electrical generator operates. But, in a superconductor, the induced currents exactly mirror the field that would have otherwise penetrated the superconducting material, causing the magnet to be repulsed. This phenomonon is known as diamagnetism and is today often referred to as the "Meissner effect" [9].

The Nb superconductors, NbTi and Nb_3Sn, are the most widely used superconductors today. NbTi has a Tc of 10 K with an Hc (4.2 K) of 12 T. In addition, it has more attractive metallurgical and mechanical properties than Nb_3Sn. Nb_3Sn has a Tc of 18 K and has an Hc (4.2 K) as high as 28 T.

American physicsts John Bardeen, Leon Cooper and John Schrieffer studied the first widely-accepted theoretical understanding of superconductivity in 1957. Their theories of superconductivity became known as the BCS theory. However, the BCS theory has subsequently become inadequate to fully explain how superconductivity occurs at higher temperatures and in different superconductor systems [9]. Brian D. Josephson predicted that electrical current would flow between two superconducting materials, even when a non-superconductor or an insulator separates them in 1962. This tunnelling is today known as the "Josephson effect" and has been applied to electronic devices such as the SQUID, an instrument capable of detecting very weak magnetic fields [10].

Another significant theoretical advancement came in 1986, a truly breakthrough discovery was made in the field of superconductivity. Alex Müller and George Bednorz created a brittle ceramic compound that superconducted at 30 K, the highest temperature then known. The Lanthanum, Barium, Cooper and Oxygen compound that Müller and Bednorz synthsized. The discovery of this was the first of the superconducting copper oxides (cuprates). This was the first of the now famous copper oxide superconductors that are known for their high Tc and Hc values, as well as highly anisotropic crystal structures. In the following years the maximum Tc was raised twice with the discovery of $YBa_2Cu_3O_{7-x}$ (Tc = 90 K) and the BiSrCaCuO (BSCCO) superconductors. The two most interesting phases of BSCCO are the $Bi_2Sr_2Ca_2Cu_3O_{10+x}$ (Tc = 110 K) and the $Bi_2Sr_2CaCu_2O_{8+x}$ (Tc = 80 K) phase, known simply as Bi-2223 and Bi-2212, respectively. Both $YBa_2Cu_3O_{7-x}$ (YBCO) and Bi-2223 have Hc (4.2 K) values greter than 100 T [11, 12].

Recent years have also seen the discovery of the first high temperature superconductor that doesn't contain any copper and the first all-metal perovskite superconductor. Also in 2001 a material that had been sitting on laboratory shelves for decades was found to be an extraordinary superconductor. A promising new HTS "Magnesium Diboride (MgB_2)" was discovered in 2001 by a team of Japanese materials researchers measured the transition temprature at 39 K for above the highest Tc of any metal or binary alloy superconductors. While 39 K is still well under the Tc's of "warm" ceramic superconductors, subsequent refinements in the way MgB2 is fabricated have opened to door to its use in industrial applications. Although it has a Tc of only 39 K, it is cheap and less brittle than other HTS materials [9].

2.2 Zero Resistance

Superconductors have zero resistivity and the magnetic field inside a bulk sample is zero. Two fundamentally important and intuitively startling properties are associated with superconductivity:

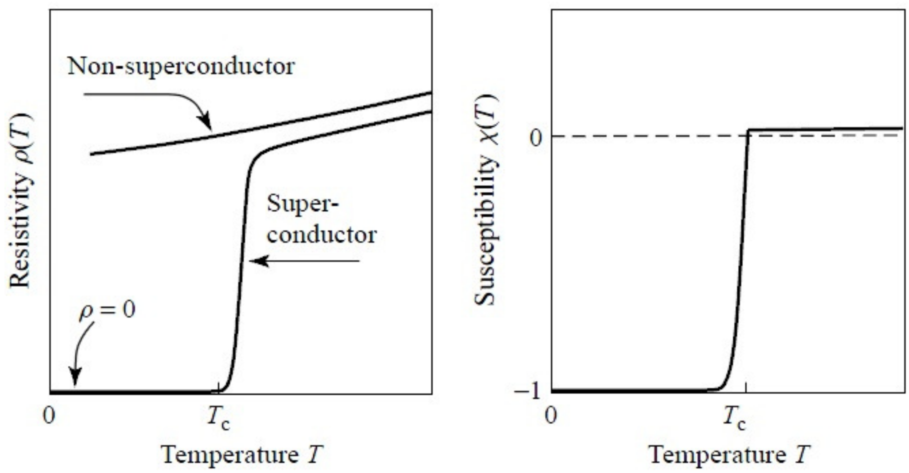

Fig. 2.1 Sketches of the two basic characteristics of a superconductor: The left figure shows the drop to zero resistivity, $\rho = 0$, at a temperature Tc, compared to a nonsuperconducting behavior. The right hand figure shows the corresponding drop in susceptibility to the ideal diamagnetic value of $\chi = -1$ below Tc. The onset of the diamagnetic response corresponds quite closely to the point where $\rho \to 0$ on the temperature axis. The figure also indicates that χ is positive but quite small above Tc [13].

i) The transition from finite resistivity, ρ_n in the normal state above a superconducting transition temperature T_c, to $\rho = 0$, i.e. perfect DC conductivity, $\sigma = \infty$, below Tc.

ii) The simultaneous change of magnetic susceptibility χ from a small positive paramagnetic value above T_c to $\chi = -1$, i.e. perfect diamagnetism below T_c. Fig. 2.1

Superconductors are materials that exhibit zero resistivity below a critical temperature (Tc), which depends upon the material. H. Kammerling-Onnes [6] first demonstrated it in 1911 with his finding that resistance of mercury dropped to zero held at or below 4 K. This sudden drop in resistance, shown in Figure 2.2, is charecteristic of all superconductors. A number of metals besides mercury (including tin and lead, but not including magnetic metals or very good normal conductors such as copper and gold), as well as certain alloys and intermetallic compounds were also soon found to be superconducting at similar low temperatures [14]. The superconductor expels magnetic flux from its interior when cooled below Tc in a magnetic flux density less than Bc (the Meissner effect) [15].

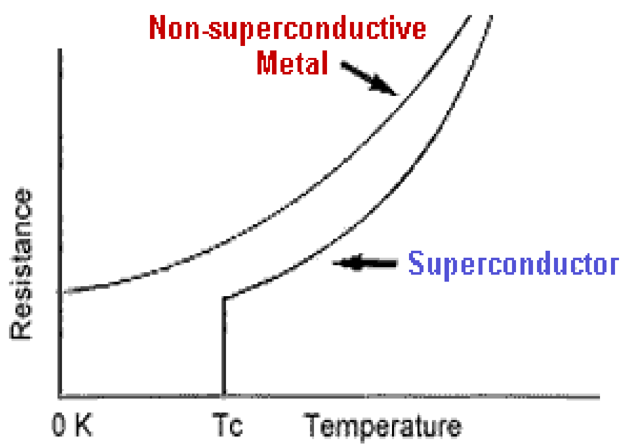

Fig. 2.2 The critical temperature dependence of resistance of a normal metal and a superconductor.

2.3 Magnetic Properties

Superconducting materials have interesting magnetic properties so that they behave as perfect diamagnets when an external magnetic field is applied. Eddy currents in the superconductor induce a magnetic field which exactly cancels the applied magnetic field within the bulk of the superconductor.

Figure 2.3 shows induction field lines near normal and superconducting samples in identical applied magnetic fields (Meissner Effect).

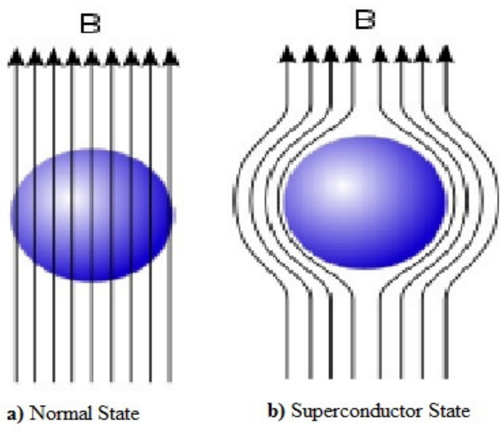

Fig. 2.3 Meissener effect in a superconducting sphere cooled in a constant applied magnetic field; on passing below the transition temperature the lines of induction B are ejected from the sphere.

2.3.1 Perfect Diamagnetism and Meissner Effect

Flux exclusion is not complete near a sample surface. Rather, the induction field decays exponentially with distance into the sample. The characteristic penetration depth is typically a few hundred angstroms.

Current exists at the surface of superconductors in a magnetic field, but not in its interior. According to the steady state Maxwell equation $\nabla \times B = \mu 0 J$, so $J = 0$ in the interior of a field free region. On the other hand, surface current creates an induction field that cancels the applied field in the interior and augments it in the region just outside the surface. Here B is the applied magnetic field, J is the current density. The critical current density (Jc) of bulk ceramic superconductors is often several orders of magnitude lower than that of a single crystal or oriented film of the some material due to the weak links residing of the boundaries between single crystals within the ceramic sample.[16]

In 1933 Meissner and Oschenfeld made a remarkable discovery that when a superconductor is placed in a magnetic field which is less than the so-called critical magnetic field, the superconductor generates spontaneous diamagnetic currents expelling the magnetic field completely from the bulk of the material.[7]

The Meissner Effect has remarkable implications. Consider a cylinder of material which is superconducting below Tc. If the temperature is initially above Tc, application of a steady magnetic field B will result in full penetration of the field into the material. If the temperature is now reduced below Tc, the internal field must disappear. This implies the presence of a surface current around the cylinder such that the resulting solenoidal field exactly cancels the applied field throughout the volume of the rod. A current in a long solenoid produces a uniform field inside the solenoid parallel to the axis with a magnitude determined by the surface current density (current per unit length along the solenoid axis), and no field outside the solenoid. In the case of the superconducting cylinder in a magnetic field, the surface current is in a surface layer with a thickness of the order of λ_L.[17]

When a material makes the transition from the normal to superconducting state, it actively excludes magnetic fields from its interior (Fig. 2.4). Meissner and Ochsenfeld managed to escape this conceptual trap by observing that a magnetic field, which was applied above Tc would be expelled from the body of the superconductor on cooling below Tc, leading to $B = 0$ inside. Using the constitutive equation for a magnetic body we therefore have to write, in the superconducting state:

$$B = \mu_0(H + M) = 0 \qquad (2.1)$$

which means that *in* the superconductor

Therefore, the susceptibility takes on the ideal value for a perfect diamagnet:

$$\chi = \frac{dM}{dH} = -1 \qquad (2.2)$$

Because permeability is $\kappa = 1 + \chi$ we also have $\kappa = 0$ below T_c.

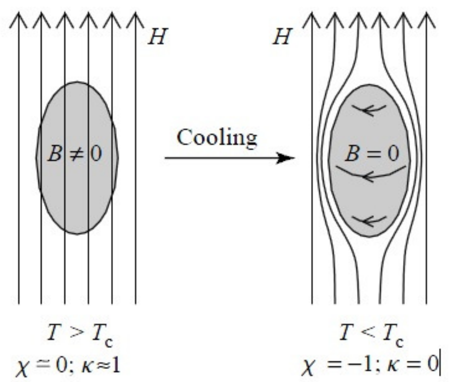

Fig. 2.4 The Meissner effect; For $T > T_c$ or $H > H_c$, normal conductor, $T < T_c$ and $H < H_c$, material is superconductor.

The Meissner effect is the repulsion of a magnetic field from the interior of a superconductor below its critical temperature. Whereas a weak magnetic field is totally excluded from the interior of a superconductor, strong magnetic fields will penetrate the material and can currently lower the critical transition temperature of the superconductor [6-9].

It is necessary to underline that all of superconductors behave as a perfect diamagnet, expelling all applied magnetic flux, up to a materials specific limit of critical magnetic field.

2.3.2 Critical Magnetic Field

If the magnetic field applied to a superconductor is sufficiently strong, it destroys superconductivity and the sample becomes normal. As a result of this, superconductors can be divided into two classes according to their behaviour in a magnetic field. These are Type 1 and Type 2 superconductors.

2.3.2.1 Type I Superconductors

The Type I category of superconductors is mainly comprised of metals and metalloids that show some conductivity at room temperature. Type I superconductors characterized as the "soft" superconductors-were discovered first and require very low temperatures to become superconductive. They exhibit a very sharp transition to a superconducting state and "perfect diamagnetism" the ability to repel a magnetic field completely [18].

High purity samples of lead, mercury and tin are examples of Type-I superconductors. Type I superconductors have critical fields too low to be used in superconducting magnets. The strongest type I pure lead has a critical field about 800 gauss.

Critical fields for type I superconductors are temperature dependent. In a type-I superconductor, the superconducting state collapses at the thermodynamic critical field Hc and the applied field enters the material. But if the field is now reduced the material re-enters the superconducting state at the same field, and the flux which had entered is expelled. This expulsion of the flux is the Meissner effect. The expulsion of the field increases the energy of the system and the work required comes from condensation into the superconducting state.

The superconductor switches abruptly over from the Meissner state to one of full penetration of magnetic flux, the normal state, at a well-defined critical field, Hc. Examples of such materials are Hg, Al, Sn, In. Figure 2.5.(a) shows a sketch of this behaviour. The ideal behaviour is only observed when n = 0.

In Type I superconductors, superconductivity is abruptly destroyed when the strength of the applied field rises above a critical value Hc. Depending on the geometry of the sample, one may obtain an intermediate state consisting of regions of penetrated magnetic flux mixed with superconducting regions containing no field.

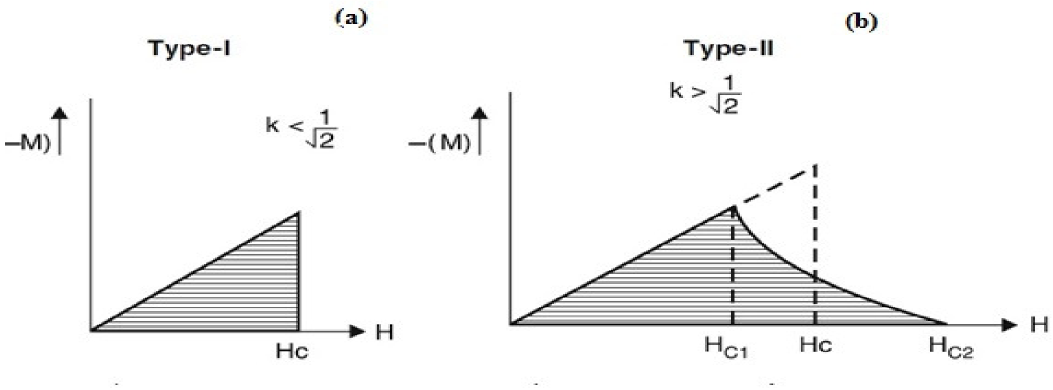

Fig. 2.5 Magnetisation versus applied magnetic field for (a) type-I and (b) type-II superconductors.

2.3.2.1 Type II Superconductors

This is also called "High-Tc superconductor". Two critical field points are important for type II superconductor. These are H_{c1} and H_{c2}. The figure 2.5 (b) shows the variation of the magnetization as a function of the applied magnetic field.

The material exhibits the full Meissner effect below Hc_1 but between Hc_1 and Hc_2, magnetic flux penetrates and the material consists of normal and superconducting regions. This is known as the mixed state, the material still superconducts, but is a mixture of normal and superconducting phases. Type-II superconductors also known as the “hard” superconductors differ from Type-I in that their transition from a normal to a superconducting state is gradual across a region of “mixed” state behaviour. A type-II will allow some penetration by an external magnetic field into its surface [19].

High values of Jc can be achieved in Type II materials with introducing a high density structural defects; such as normal precipitates, grain boundaries and dislocations [20].

Most pure elemental superconductors (except niobium, technetium, vanadium and carbon nanotubes) are Type I, while almost all impure and compound superconductors are Type II. This is also called “High-Tc superconductor”. Two critical field points are important for type II superconductor. These are Hc_1 and Hc_2. Figure 2.6 indicates the variation of the magnetization as a function of the applied magnetic field.

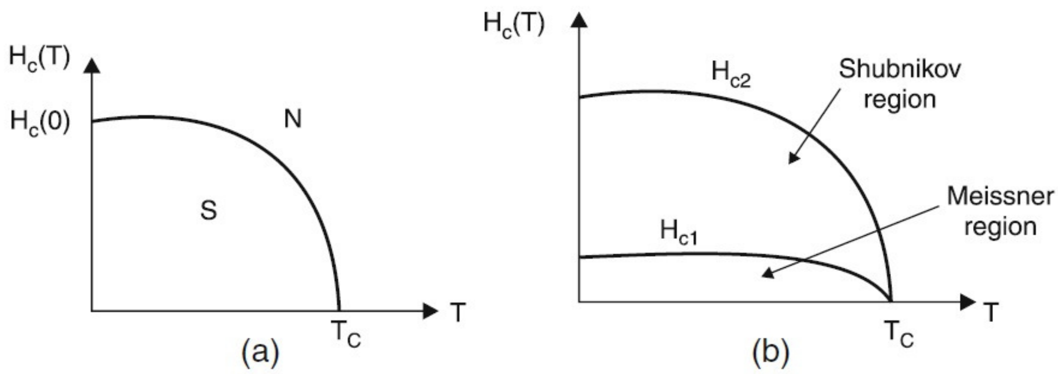

Fig. 2.6 Critical magnetic field as a function of temperature for (a) type-I and (b) type-II superconductors.

It can be concluded that raising the applied field above a critical value Hc_1 leads to a mixed state in which an increasing amount of magnetic flux penetrates the material, but still the material can carry resistanceless current as long as the current is not too large in type II superconductors. At a second critical field strength Hc_2, superconductivity is totally destroyed. The mixed state is actually caused by vortices in the electronic superfluid, sometimes called "fluxons" because the flux carried by these vortices is quantized.

2.4 Penetration Depth and Coherence Length

The external magnetic field falls off exponentially such as one moves into the superconductor due to the shielding effect. The depth to which magnetic field penetrates the superconductor is called the penetration depth. This is an experimental quantity and depends on the absolute temperature, the penetration depth at 0 K being λ_0 [15].

$$B(x) = B_0 \, e^{-x/\lambda} \tag{2.3}$$

The variation of the magnetic field inside a semi-infinite type I superconductor with distance is plotted in Figure 2.7. The superconductor possesses the region on the positive side of the x axis. The magnetic field exists very small at depth a few times λ below the surface. The expulsion of the magnetic field is accomplished by shielding supercurrents which flow at the surface of the superconductor without any Ohmic losses. These supercurrents form a finite sheath and spread out to a thickness λ_L [15].

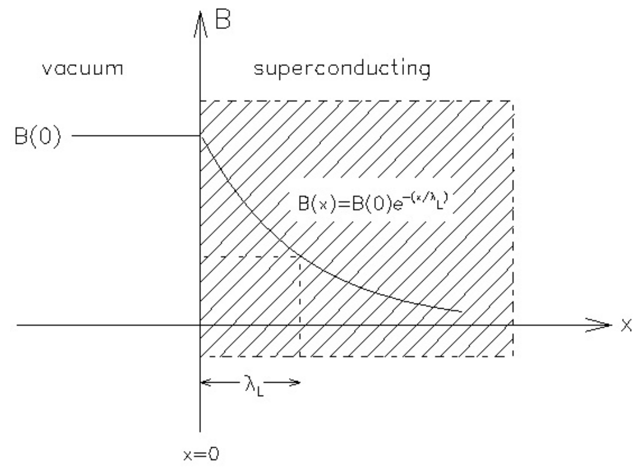

Fig. 2.7 The magnetic field B inside a semi-infinite superconductor versus distance x from its surface. The field outside the superconductor (for x< 0) is B_0, and the superconductor is to the right of the dashed line

The "London" name comes from brothers F. London and H. London, who created a theoretical model of superconductivity in 1935. For a more technical explanation and the actual formula to calculate penetration depth;

$$\lambda = (m/\mu_0 n_s e^2)^{1/2} \tag{2.4}$$

The coherence length is defined as an independent characteristic length. It is related to the Fermi velocity for the material and the energy gap associated with the condensation to the superconducting state. It has to do with the fact that the superconducting electron density cannot change quickly. There is a minimum length over which a given change can be made, lest it destroy the superconducting state [21]. For instance, a transition from the superconducting state to a normal state will have a transition layer of finite thickness which is related to the coherence length. Experimental studies of various superconductors have led to the following calculated values for these two types of characteristic lengths.

In other words, addition of impurities increases the penetration depth and decreases the coherence length. As a result, the material undergoes at transition from type I to type II superconductor. Both coherence length and penetration depth diverge in the same way near $T = T_c$. So, a constant k is defined as $k = \lambda/\xi$, which will remain finite as $T \rightarrow T_c$. This is known as *Ginzberg–Landau parameter* and can be considered as a characteristic of a material [13].

2.5 BCS Theory

Electrons are bound together in pairs by an electron-phonon interaction in superconductors. The cooper pairs, or the presence of superconducting electrons in the material, tends to lead to the formation of more bound pairs. These cooper pairs are bosons and can therefore have the same energy state.

An electron in a solid passing by adjacent ions in the lattice can act on these ions with a set of coulomb attractions which gives each of the ions momentum that leads the ion to move together on a small region. Because of the elastic properties of the lattice, this region of increased positive charge density will than propagate as a wave, which carries momentum, through the lattice. The electron has emitted a phonon. The momentum of the phonon carriers is supplied by the electron, whose momentum was changed when the phonon was emitted. If a second electron subsequently passes by the moving region of increased positive charge density, it will experience an attractive Coulomb interaction, and thereby it can absorb all the momentum the moving region carries. It means that the second electron can absorb the phonon by absorbing the momentum supplied by the first electron. The net effect is that the two electrons have exchanged some momentum with each other and thus they have interacted with each other.

All the cooper pairs in a superconductor can be described by a single wave function. This has a very long wavelength, and thus electron pairs are not scattered by those defects which are efficient at scattering normal electrons which implies zero resistance to the flow of a dc electrical current. It is necessary to know that the other properties of superconducting materials, such as the coherence length and penetration depth, must be considered to determine how the microstructure will affect the superconducting [22].

Consequently, the BCS theory shows that in certain conditions the attraction between two electrons due to a succession of a phonon exchange can exceed slightly the repulsion which they exert directly on each other because of the (shielded) Coulomb interaction of their like charges. Then the electrons will be weakly bound together, and form is called as cooper pair. So the cooper pairs are responsible for superconductivity [23].

CHAPTER 3

REVIEW OF HIGH TEMPERATURE SUPERCONDUCTORS

3.1 Introduction

After the discovery of liquid helium, Kamerling Onnes discovered that the electrical resistance of Hg decrease to small undetectable values under a certain critical temperature (Tc) in 1908 [6]. It means that the superconductivity was discovered. The highest Tc was measured at 23.2 K for Nb3Ge compound. Moreover, the BCS theory explains that superconductivity microscopically as electron-lattice-electron interaction theoretically predicted maximum critical temperature about 30-35 K for superconductors. High electrical conductivity was first discovered in 1954, in perylene bromine complex. Much later the discovery of a pronounced conductivity peak in (TTF)(TCNQ) near 60K in 1973 stimulated a lot of effort in the direction of low-dimensional systems, so-called charge transfer salts.

A perovskite ceramic material was found to superconduct at 90 K in 1987. This discovery was very significant because it became possible to use liquid nitrogen as a coolant because they superconduct at significantly higher temperatures than conventional superconductors.

The discovery of the high temperature superconductors (HTS) aroused tremendous excitement since they can carry significant current above the boiling point of liquid nitrogen at 77 K [24].

After the discovery of the superconducting ceramic system La-Ba-Cu-O with critical transition temperature between 30-40 K, other families of cooper-oxide based ceramics have been synthesized with higher critical temperatures. These oxides include the Y-Ba-Cu-O series (Tc ~90 K), the Bi-Sr-Ca-Cu-O series (Tc ~80-115 K), the Tl-Ba-Ca-Cu-O group (Tc ~85-125 K), and some others which do not form obvious classes.

The high-temperature superconductors are ceramic materials having copper-oxygen planes. Such planes are believed to play an important role in the mechanism of superconductivity. Transition temperatures of the ceramic superconductors depend on the charge carrier concentration in the Cu-O planes. High temperature superconductors are Type II superconductors having extremely high critical magnetic fields, Hc2. Their properties are very anisotropic; properties are quite different in different crystalline directions. The coherence length of these superconductors is very short.

3.2 The Crystal Structure of BSCCO

Structural features play an important role for superconductivity in HTSCs. Therefore, it is useful to consider structural parameters that affect transition temperature. It is parameters and geometry of theses planes that affect Tc. For instance, in the case of mercury compound the influence of Cu-O length on Tc is well demonstrated and the highest Tc corresponds to the shortest Cu-O bond.

All ceramic superconductors are composed of similar building blocks, which can be closely related to the classic perovskite ABO_3 Structure. In the following sections the crystal structure and superconducting properties of the yttrium based and bismuth based superconductors are presented.

$Bi_2Sr_2Ca_{n-1}Cu_nO_{2n+1}$ is the general form of Bi-based superconductor compounds where n=1, 2, 3 gives the number of CuO_2 layers. This system is usually called as BSCCO and known superconducting phases are the (2201), (2212) and (2223) phases, with the critical temperatures of 20 K , 85 K and 110 K respectively. In the high-Tc 2223 phase, it is difficult to achieve a single phase using a solid state reaction of raw material mixtures having starting composition of the high-Tc phase.The crystal structures of three phases of the Bi-based superconductors are illustrated in figure 3.1.

An acronym for a ceramic superconductor system containing the elements Bismuth, Strontium, Calcium, Copper and Oxygen. Typically, a small amount of lead is also included in these compounds to promote the highest possible Tc. BSCCO has probably found the widest acceptance among high-Tc superconductor applications due to its unique properties. BSCCO compounds exhibit both an intrinsic Josephson effect and anisotropic (directional) behavior [25].

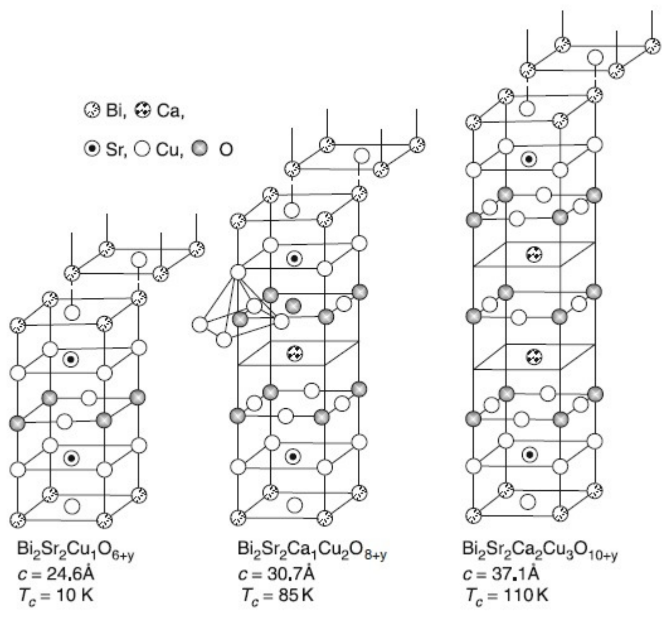

Fig. 3.1 The crystal structures of the Bi phases of general formula $Bi_2Sr_2Ca_{n-1}Cu_nO_y$ with n=1, 2 and 3

The superconducting properties are very anisotropic and structure sensitive and it is difficult to obtain high density BSCCO ceramics by conventional sintering [26, 27].

The current voltage characteristic (IVCs) of the BSCCO tapes showed a strong temperature dependence becoming shallower as the temperature falls. The apparent critical current of the tape is strongly dependent on the voltage criteria that is adopted to define the onset of dissipation [28].

The Bi-Sr-Ca-Cu-O system has a layered crystal structure. The crystal structure of each of these phases consists that two displaced Sr-Bi-O-Sr layers separated by Ca-Cu-O layers. Generating the high Tc phase usually requires the use of lead or antimony to rise the rate of reaction with a flux growth mechanism, and mechanical mixing between heat treatments. On the other hand, BSCCO demonstrates anisotropic growth, with growth preferentially occurring along the (100) direction, the direction of a-b planes. However, this physical property can be utilised to produce aligned crystals with the conduction planes all parallel thereby improving the Jc characteristic. For BSCCO at low temperatures the critical current density is determined by the strength of flux pinning, but at temperatures above about 20K flux creep is dominant and the current capacity is significantly reduced by flux creep [29].

3.3 Common Properties of the Copper Oxide Superconductors

All cuprates have some features in common. The most important feature of the copper oxide superconductors is to have a layered crystal structure consisting of one or more Cu-O planes. The Cu-O planes are considered to conduct supercurrent. The transition temperatures of these superconductors are closely correlated with the number of Cu-O layers in the unit cell, and the charge carrier concentration in the layers. The Cu-O layers are separated by arrays of other atoms. The intervening layers can be divided into two categories: structural layers and charge reservoirs. The structural layers, like Y layer in YBCO, play a minor role in the variation of the Tc, but the charge reservoir layers have a large impact on Tc. The distance between CuO_2 planes and the charge reservoir layers, which provide the charge carriers into Cu-O planes is also important. The crystal structures of the HTSCs are all anisotropic. The anisotropy of the crystal structure manifests itself in the electrical conduction, with high-conductivity in the Cu-O planes.

CHAPTER 4

PRODUCTION OF SAMPLES AND EXPERIMENTAL MEASUREMENT SYSTEM

4.1 Preparation Powders of $Bi_{2-x}Sr_{1.9}Ca_{2.1}Cu_{3.2}Sm_xO_y$

Superconducting samples $Bi_{2-x}Sr_{1.9}Ca_{2.1}Cu_{3.2}$ Sm_xO_y were prepared by the standard solid-state reaction method. The solid state reaction method is a general method to produce HTSCs. The process consists of selection of raw materials, weighing, mixing, calcining and pulverizing steps. The weighed powders of Bi_2O_3 (99.99%), PbO (99.9+%), $SrCO_3$ (99.9+%), $CaCO_3$ (99+%) and CuO (99+%) in the cation ratio of Bi: Sr: Ca: Cu = 2: 1.9: 2.1: 3.2 were troughly mixed by ball grinding for 24 h. Samarium ions are substituted with Bismuth ions as x=0, 0.01, 0.03, 0.05, 0.07, 0.1 and 0.3 in this experiment. After milling, the mixed powders were calcined in air at temperatures of 750, 800 and 840°C for 24 hours durations. The powder was ball milled after each calcinations step. The calcined material was pressed into pellets at 200 MPa. A rectangular pressing die is used for pelletization. The pelletized samples were sintered in air at various annealing temperatures for the durations of 24 hours. Throughout our experiments, the heating and cooling rates of the temperature were chosen to be 10 and 3°C min^{-1}, respectively.

4.2 XRD Measurements

The diffraction data which depends on the lattice parameters is unique for a particular material and can be employed in the identification of a material, just as fingerprints are used to identify a human being. X-ray is that part of the electromagnetic spectrum which covers the wavelength range 0.1-200A. Only a relatively small part of the total X-ray region is covered by the conventional X-ray spectrometer. The X-rays used for the material characterization is CuKo. whose wavelength is 1.5418A The basic principle involved in the X-ray studies is the Bragg's law *i.e.,* $n\lambda$ = 2dsinΘ, where Θ is the glancing angle at which the X-ray strikes the surface of the crystal, A is the wavelength of the X-ray used, n (an integer) is the order of diffraction and d_{hkl} is the distance between the parallel planes having miller indices *h, k, I.* The lattice parameters a, b and c can be calculated by indexing the sharp peaks (assigning *h, k, I* values) and using the equation;

$$dhkl = 1 / \sqrt{[(h^2) + (k^2) + (l^2)]} \tag{4.1}$$

In polycrystalline samples or powder of a crystalline material, the crystals are randomly oriented. If such a sample is struck by an X-ray beam, there may be many planes which are oriented in such a way that Bragg's law is satisfied and we obtain a resultant diffraction pattern with peaks corresponding to all such planes. In order to ensure that more number of planes are exposed, the sample is rotated by an angle 0 on its own axis during exposure. The diffracted beams are collected by scintillating counter, which acts as a detector, at an angle 28. This output is fed to a recorder which records the output (which is proportional to the intensity of the diffracted beam) versus 26. From the positions, relative intensities of the peaks and from the area under its profile, the position of the atoms in a unit cell can be determined. The orientation of the crystallites can also be determined from the relative intensities. The shape of the peak provides information regarding the crystallite size and lattice imperfections including strains.

Fig. 4.1 Rigaku Multiflex+ X-Ray Diffractometer

4.3 SEM Measurements

The microstructure analysis was carried out using a JOEL JSM 6400 model scanning electron microscope operated 20kV. The microstructure of the samples are performed by looking for grain connectivity, grain size, orientation of the granular structure and the presence of microvoids. Effects of the sample preparation conditions on the microstructure were investigated by this technique [31].

Fig. 4.2 JEOL JSM-6390LV scanning electron microscope

4.4 Resistivity Measurements

R-T measurements of all samples is carried out using 4 probe arrangement. The temperature dependent resistance ρ (T) was measured using standard four-probe technique (Fig. 4.1) with a nanovoltmeter. Contacts were made with thin copper wires using silver paint. The contacts were received on the same surface and were equal to the distance between contacts because of minimize measurements errors. The current was applied to the two outer electrical contacts. Then, the voltage drop across the two inner electrical contacts was measured against temperature. To convert voltage to resistivity, the calculation is made as following:

$$\rho = \frac{(V)(A)}{(I)(l)} \tag{4.2}$$

where, ℓ is the distance between the inner electrical contacts, A is cross-section area of the sample.

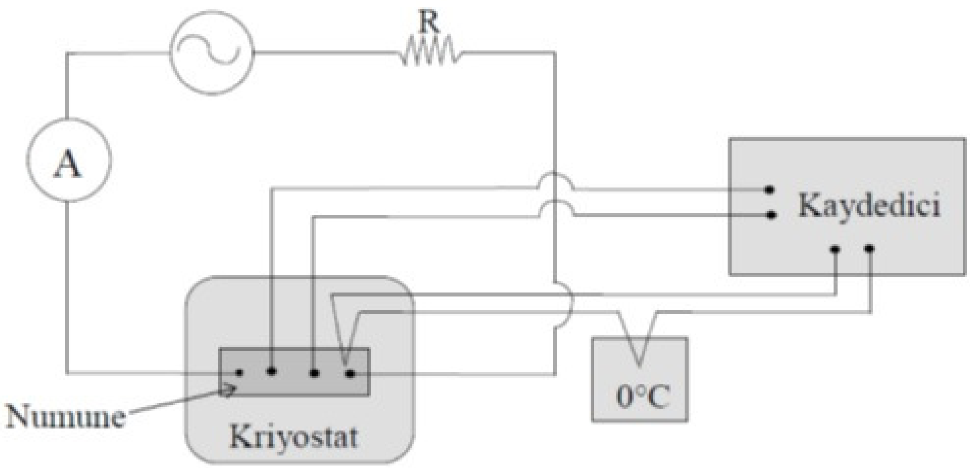

Fig. 4.3. The figure of R-T Measurements by using four-probe method

Fig. 4.4 Cryostat System

The zero resistance transition temperatures were determined from the resistance versus temperature graphs. The resistance versus temperature graph usually shows a sharp rise in resistance by increasing temperature above Tc, and then exhibits a linear increase with temperature.

4.5 Microhardness Measurements

The Vickers hardness test method consists of indenting the test material with a diamond indenter, in the form of a right pyramid with a square base and an angle of 136 degrees between opposite faces subjected to a load of 1 to 100 kgf. (Fig. 4.2) The full load is normally applied for 10 to 15 seconds. The two diagonals of the indentation left in the surface of the material after removal of the load are measured using a microscope and their average calculated. The area of the sloping surface of the indentation is calculated. The Vickers hardness is the quotient obtained by dividing the kgf load by the square mm area of indentation.

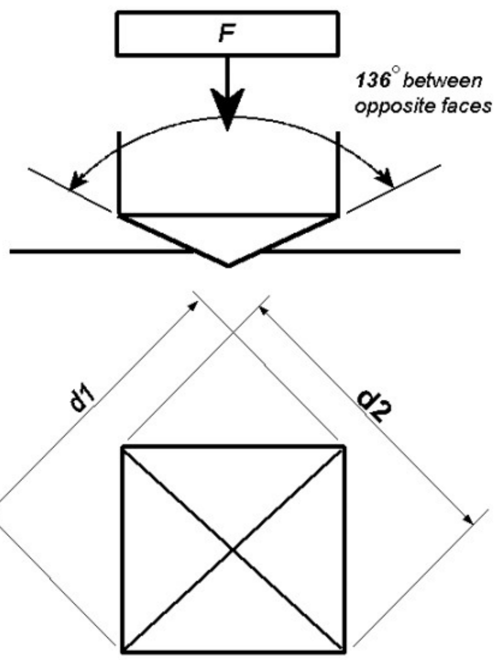

Fig. 4.5 The figure of Microhardness Measurements via Vickers Technique

The load dependent microhardness (Hv) values of various applied loads (0.245 N≤F≤2.940 N) can be extracted from the formula:

$$H_V = 1854.4\left(\frac{F}{d^2}\right) \tag{4.3}$$

here (d) is our experimentally measured indentation diagonal lengths at different applied loads (F) are visualized in Table 7. It is visible from the table that the Hv values for all the samples depend strongly on the applied loads and diffusion annealing temperature.

Further, the Young's (elastic) modulus (E) and yield strength (Y) can be evaluated from the equations:

$$E = 81.9635\, H_v \tag{4.4}$$

$$Y \approx \frac{H_V}{3} \tag{4.5}$$

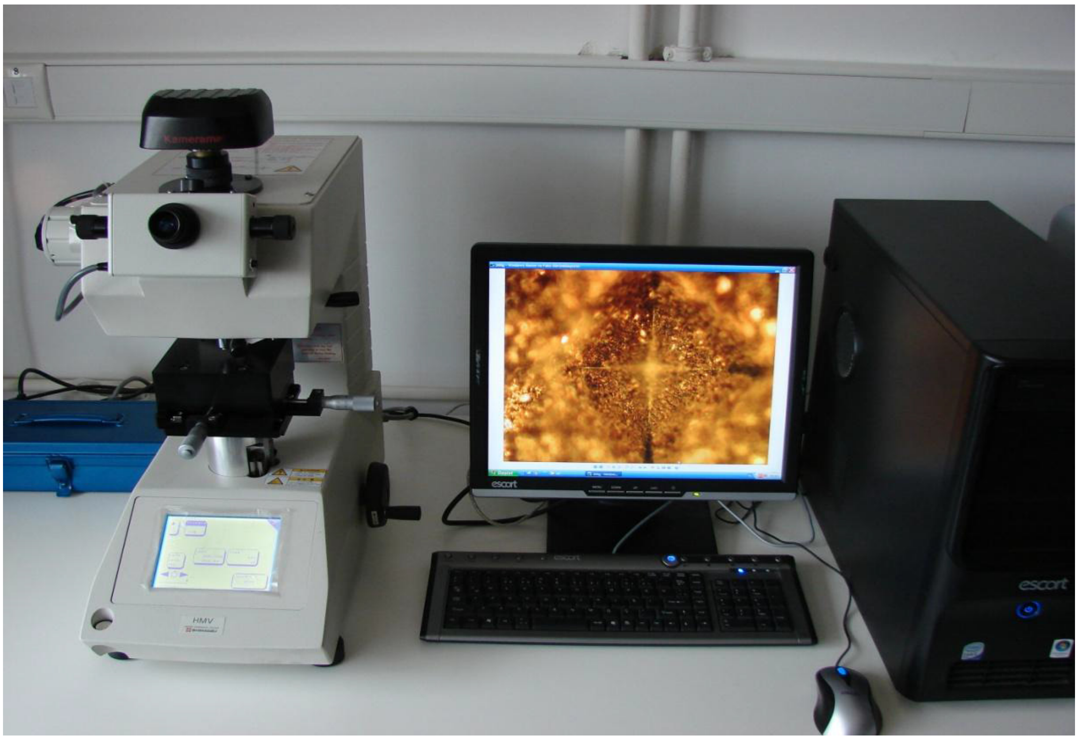

Fig. 4.6 Digital microhardness tester Shimadzu HVM-2

CHAPTER 5

EXPERIMENTAL RESULTS AND DISCUSSION

5.1 R-T Measurements Analysis

We have investigated the effect of the partial substitution of Bi by Sm in the Bi-2223 superconducting samples prepared by standard solid-state reaction method. Our investigations consisted of DC electrical resistivity, X-ray diffraction (XRD) and scanning electron microscopy (SEM) measurements. We measured the critical transition temperatures, activation energies and irreversibility lines from the resistivity versus temperature curves under DC magnetic fields in the range of 0 and 5 T. The superconducting transition temperature Tc was shown in Table 1. Onset critical (T_c^{onset}) and offset critical (T_c^{offset}) temperatures of the samples studied are another probable results obtained from Fig. 1. The former is in accordance with the transition of isolated grains to the superconducting state whereas the latter is related to the volume fraction of Bi-2223 phase and/or features of intergranular component [32, 33]. Table 1 displays the variation of the T_c^{onset} and T_c^{offset} values deduced from Fig. 1 as a function of the Sm content to substitution with Bi in the Bi-2223 system. not only the improvement of crystallinity and increment in the grain size but the optimization of the hole concentration and possible changes in the lattice vibration of the samples studied, as well. However; from x=0.1 onwards these characteristics begin to decrease systematically towards their local minimum points, being attributed to either the reduction of the crystallite size and the hole concentration or the increment of the porosity and weak links between the grains [33, 34], which is favored by the bulk density measurements.

The critical temperature were found to increase with increasing Sm concentration and with increasing applied magnetic field until Sm concentration was 0,3. After that, the critical temperature was decreased. The residual resistance ratio was calculated from;

$$RRR = \frac{\rho_{300\,K}}{\rho_{120\,K}} \tag{5.1}$$

The maximum residual resistance ratio was observed during the concentration of Sm was 0,1.

We measured the critical current density as;

$$J_c = \frac{I}{A} \tag{5.2}$$

where I is the critical current and A is area ($A.cm^{-2}$). The sixth sample had the biggest critical current density. Critical current density (J_c) measurements are an effective method to examine the pinning mechanism of the superconducting materials [35].

The variation of $\Delta T_c (T_c^{onset} - T_c^{offset})$ is also another important point obtained from Fig. 1. The ΔT_c values inferred are depicted in Table 1. It is obvious from the table that the ΔT_c significantly reduces from 8.68K to 3.66 K with the increment of the Sm substitution with Bismuth in the Bi-2223 system up to x=0.07. In other words, from x=0.1 onwards the broadening of the resistive transition enhances with ascending the level of the Sm substitution in the Bi-2223 materials (Fig. 1) as a consequence of the existence of porosities and weak links between the superconducting grains and especially the divergence from the optimization of the hole concentration, being supported by the results of the SEM measurements [36–38].

Table 1 Resistivity measurement results for the samples studied.

Samples	T_c^{offset} (K)	T_c^{onset} (K)	ΔT_c (K)	J_c A.cm^{-2}	ρ_{300K} *(mΩ cm)*	ρ_{120K} *(mΩ cm)*	*RRR*	$\Delta\rho$
Sm0	101.31	109.99	8.68	615	19.75	10.58	1.87	9.17
Sm1	103.66	111.25	7.59	789	14.70	5.61	2.62	9.09
Sm2	104.45	111.85	7.40	801	12.99	3.98	3.26	9.01
Sm3	105.93	112.10	6.17	844	11.41	2.79	4.09	8.62
Sm4	107.37	112.78	5.41	906	9.25	1.83	5.05	7.42
Sm5	109.82	113.48	3.66	1189	6.34	0.84	7.55	5.50
Sm6	94.29	109.01	14.72	409	26.22	17.01	1.54	9.21

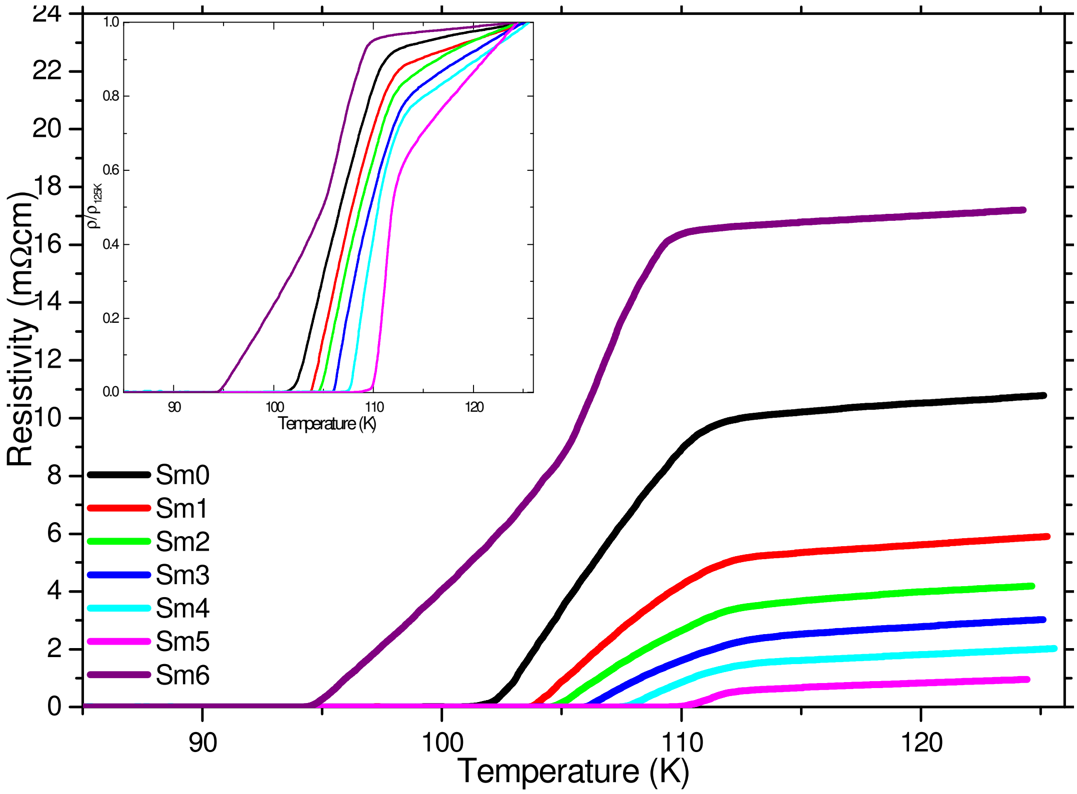

Fig. 5.1 Resistivity as a function of temperature curves for all the samples

Activation (flux pinning) energy value of a material at various applied magnetic fields can be directly estimated from the slope of linear data in the broadening tail part of Arrhenius graph [39, 40]. In [41, 42], we clearly argued the fitting of the lnρ/ρ0 versus 1/T plot called as Arrhenius graph. Fig. 3 demonstrates the nonlinear relations between lnρ/ρ0 versus 1/T plots at different applied magnetic fields for the samples produced in this work. It is obvious from the figure that the activation energy values depend on both the temperature and especially the applied magnetic field. Further, there is an exponential dependence of ρ with 1/T, indicating that the energy dissipation (the resistivity) is due to the thermal activation of flux across the pinning barrier. The current-independent resistivity can be expressed with the help of Arrhenius law [43-49],

$$\rho = \rho_0 \exp(-U_0 / k_B T) \quad (5.3)$$

where U_0 presents the activation energy value of the sample studied, kB is the universal Boltzmann's constant and ρ_0 is a field-independent pre-exponential factor.

Table 2 Activation energies and β values

Samples	***Activation Energies (K)***							β values
	0T	***0.3T***	***0.7T***	***1T***	***3T***	***5T***	***7T***	
Sm0	6982	5237	3258	2755	1610	1243	1016	0.510
Sm1	4057	3485	2456	2058	1287	1004	812	0.456
Sm2	3583	2902	2069	1762	1101	876	706	0.438
Sm3	3015	2507	1760	1526	952	787	664	0.419
Sm4	2341	1786	1217	1083	678	559	477	0.414
Sm5	1642	1064	782	670	437	361	302	0.396
Sm6	7023	5323	3261	2459	1661	1256	1008	0.525

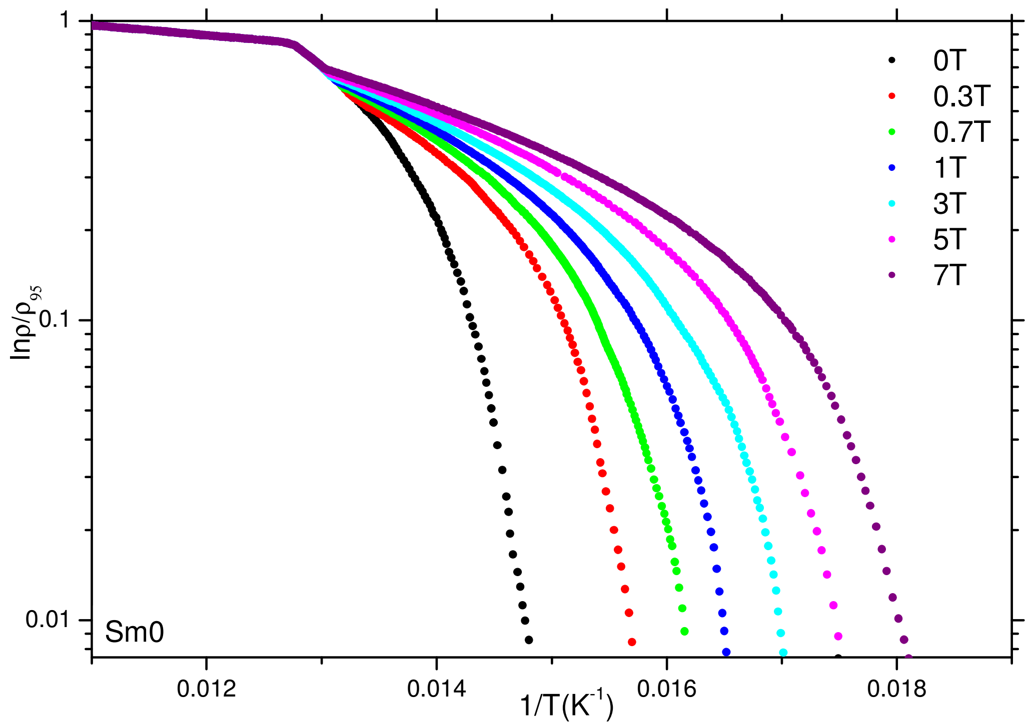

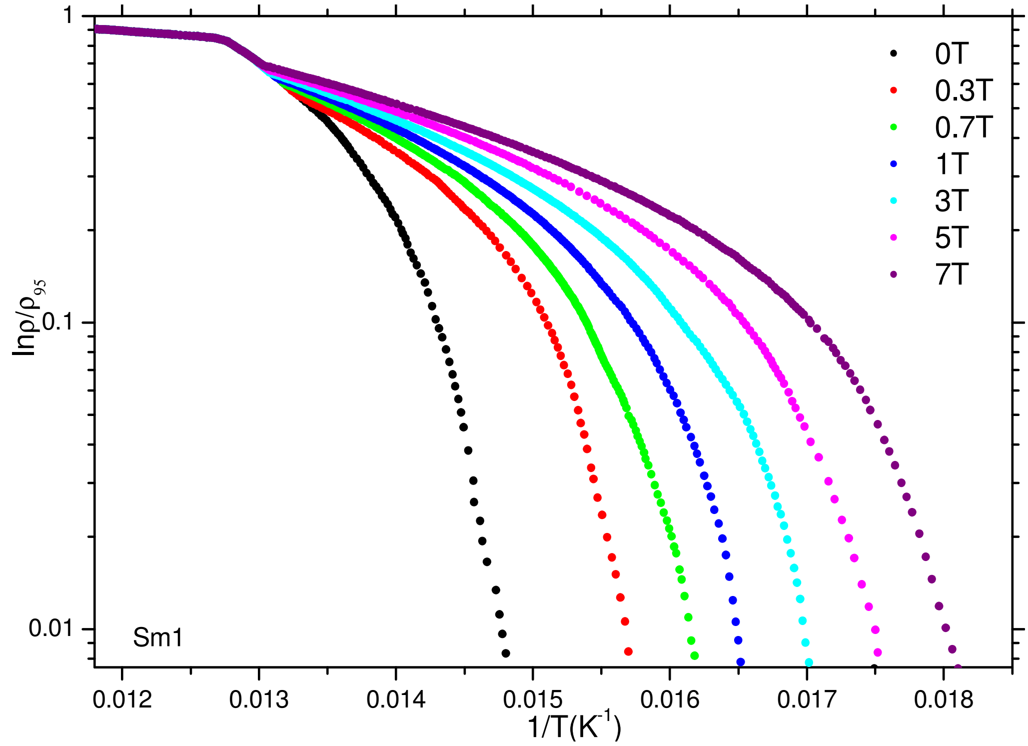

Fig. 5.2 lnρ/ρ_0 versus 1/Tgraphs of the samples. The activation energies of the samples are determined from the slopes of the linear parts of the low resistivity region.

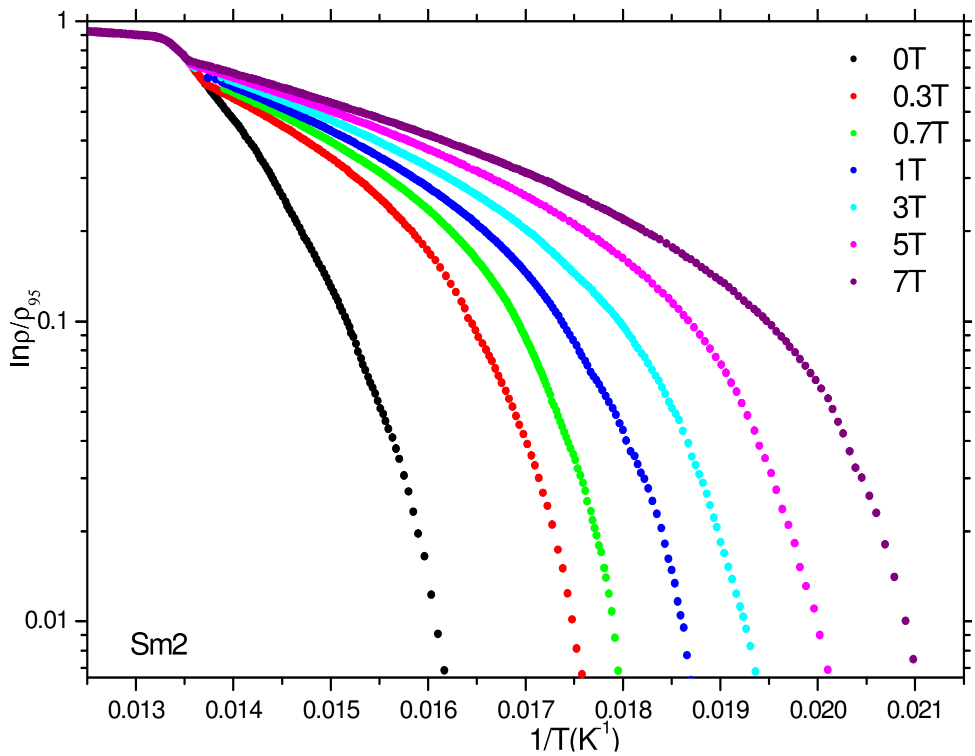

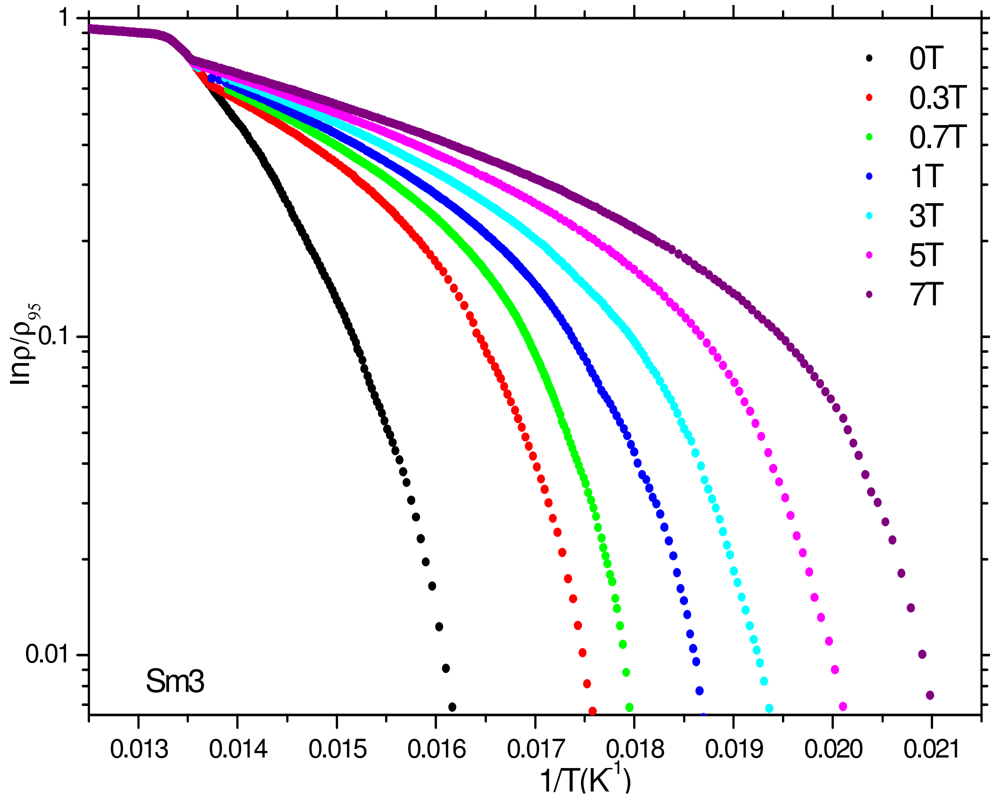

Fig. 5.2 lnρ/ρ_0 versus 1/Tgraphs of the samples. The activation energies of the samples are determined from the slopes of the linear parts of the low resistivity region (Continued).

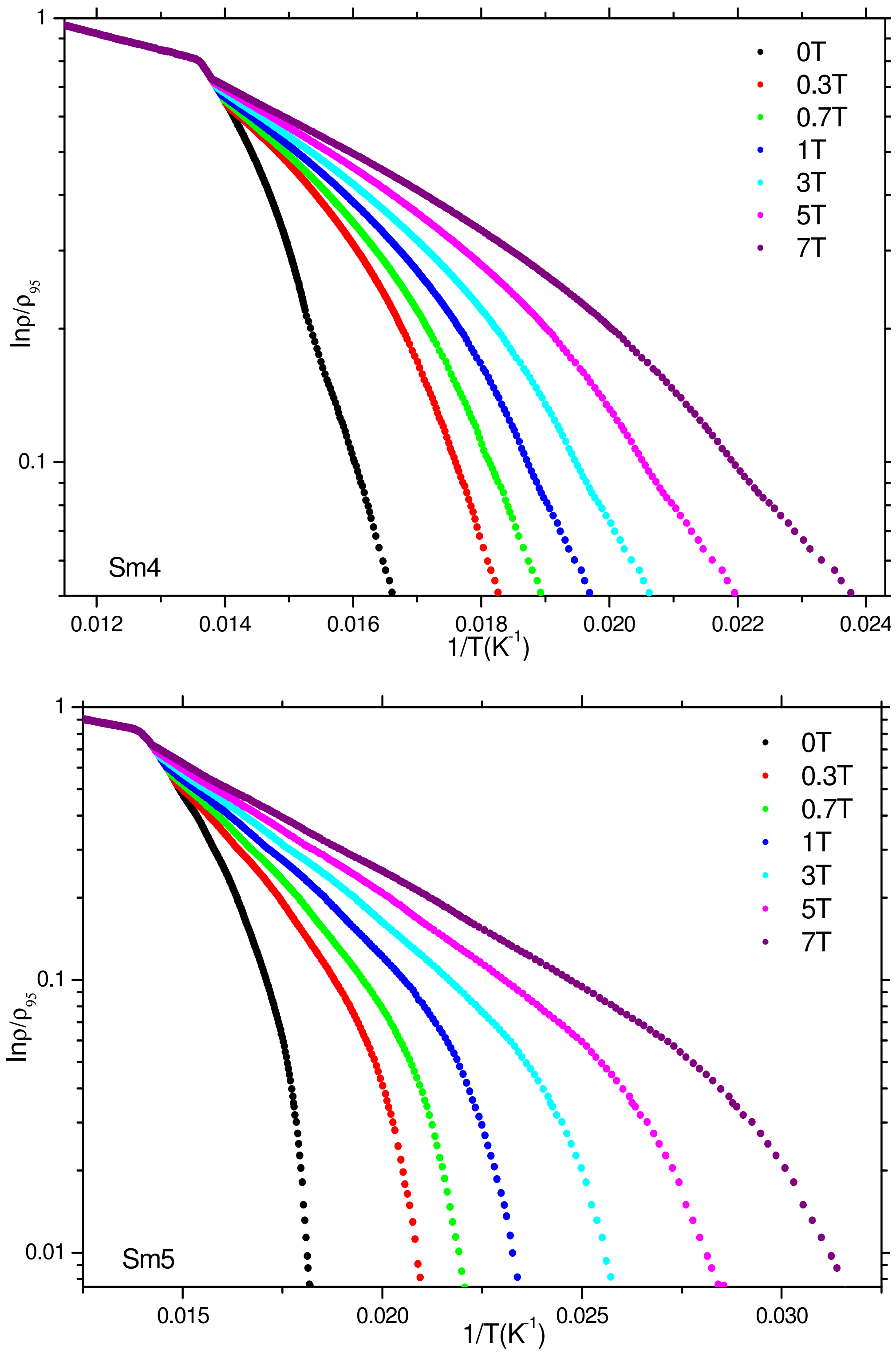

Fig. 5.2 lnρ/ρ$_0$ versus 1/Tgraphs of the samples. The activation energies of the samples are determined from the slopes of the linear parts of the low resistivity region (Continued).

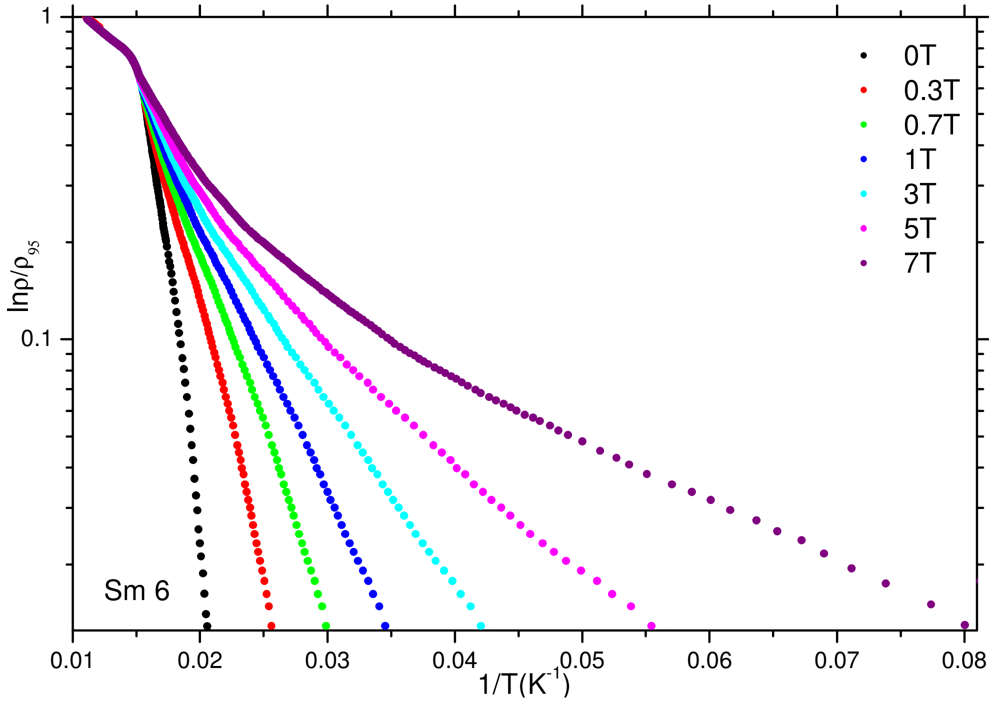

Fig. 5.2 lnρ/ρ_0 versus 1/Tgraphs of the samples. The activation energies of the samples are determined from the slopes of the linear parts of the low resistivity region (Continued).

5.2 Irreversibility and Upper Critical Field

The irreversibility fields ($\mu_0 H_{irr}$) and upper critical fields ($\mu_0 H_{c2}$) versus temperature variation for the samples are shown in Figure 5.3 and 5.4. There are several methods such as magnetization [50], critical current density (Jc) criteria of 10 A/cm^2 or 103 A/cm^2 [51, 52], plotting $J^{1/2}$ $\mu 0H^{1/4}$ versus μ_0H [53–55], resistivity criteria of 10% normal-state resistivity [56] or zero resistivity [57] to find the irreversibility field in Bi-2223 superconductors. Figure 5.3 and 5.4 demostrate both the temperature dependences of the upper critical field and the temperature dependences of the irreversibility field. The irreversibility fields decreased with increasing the applied magnetic fields in the material as shown Table 3.At the same time, the upper critical field showed that decreasing with rising applied magnetic fields as in Table 4.

Table 3 Irreversibility field values of the samples versus magnetic fields

Samples	$\mu_0 H_{irr}(T)$						
	Sm0	***Sm1***	***Sm2***	***Sm3***	***Sm4***	***Sm5***	***Sm6***
0T	84.93	94.07	98.83	98.50	102.35	106.03	74.31
0.3T	75.11	82.12	86.01	90.08	95.19	97.05	64.00
0.7T	57.31	66.84	73.13	77.98	82.78	88.06	50.15
1T	55.15	62.79	69.30	73.37	77.41	84.05	48.26
3T	50.70	57.01	63.54	68.20	72.23	76.94	44.24
5T	46.64	51.91	59.03	63.44	67.46	71.72	40.28
7T	42.19	47.19	53.96	58.41	62.64	66.32	36.38

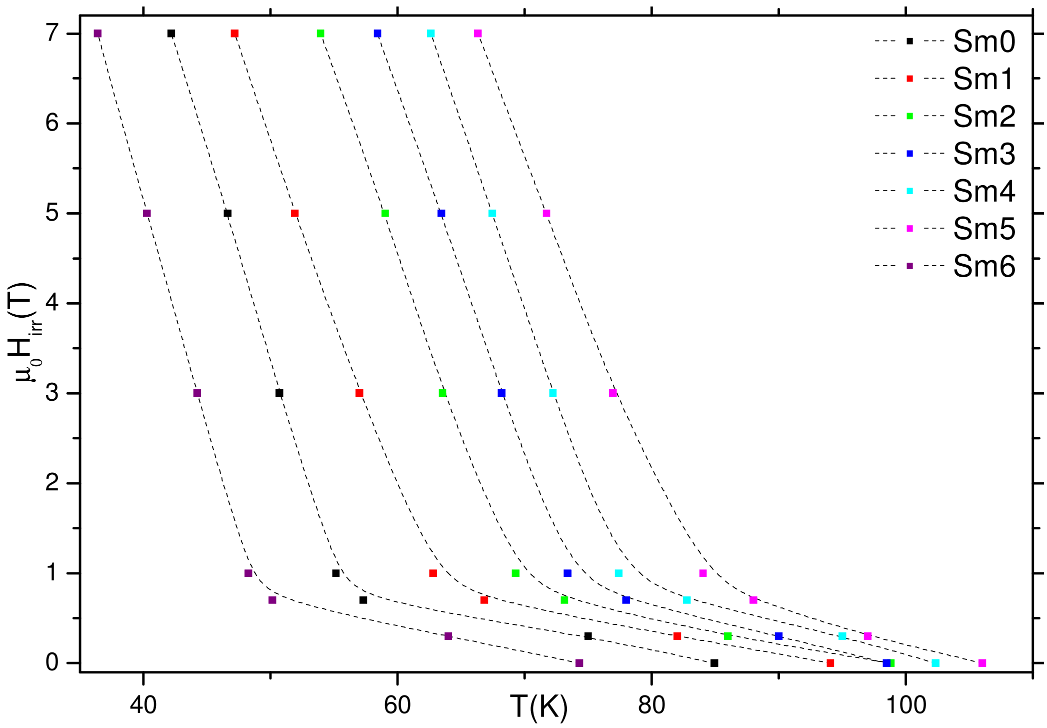

Fig. 5.3 The temperature dependences of the irreversibility field ($\mu_0 H_{irr}$)

Table 4 Upper critical field values of the samples versus magnetic fields

Samples	$\mu_0 H_{c2}(T)$						
	Sm0	***Sm1***	***Sm2***	***Sm3***	***Sm4***	***Sm5***	***Sm6***
0T	99.56	103.94	106.37	108.22	109.60	111.78	87.12
0.3T	97.33	102.30	105.38	107.42	109.05	110.99	85.17
0.7T	96.03	101.50	104.70	106.85	108.49	110.67	84.30
1T	95.25	101.03	104.38	106.62	108.21	110.48	83.90
3T	93.22	99.40	103.08	105.72	107.60	109.88	81.98
5T	91.78	97.89	102.19	104.82	107.09	109.27	80.20
7T	90.62	96.59	101.19	104.11	106.65	108.82	78.72

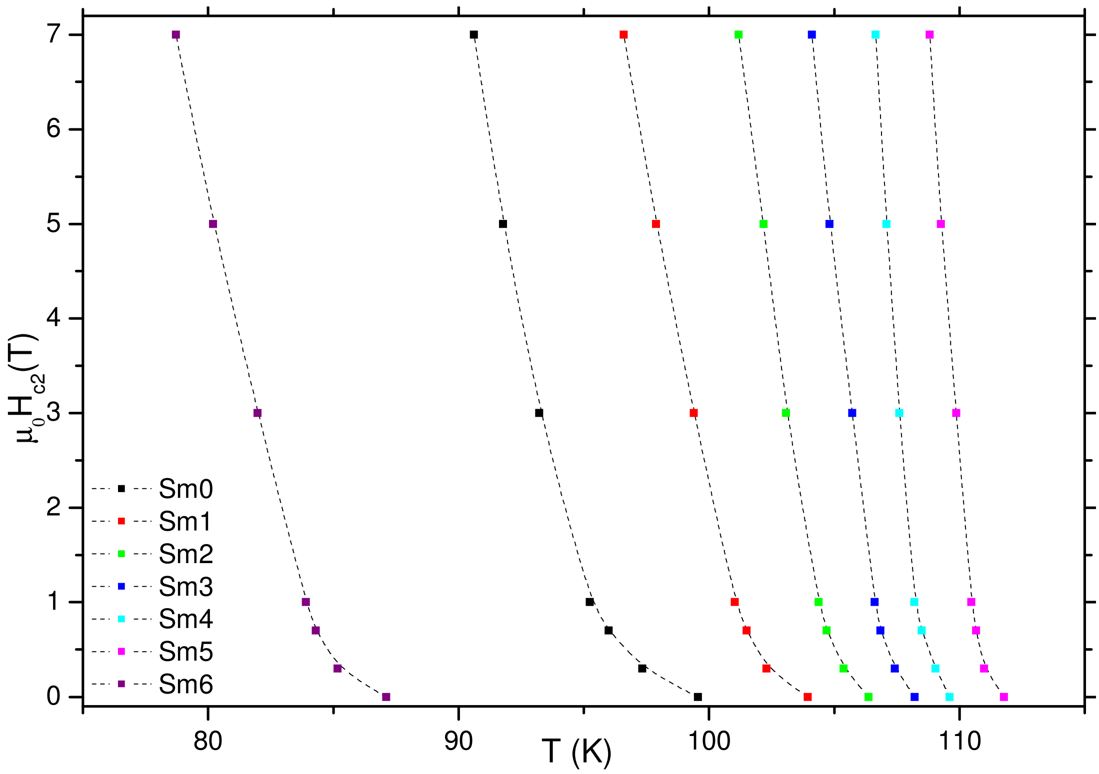

Fig. 5.4 The temperature dependences of the upper critical field ($\mu_0 H_{c2}$)

As well known, when a magnetic field applies to a superconductor it penetrates into the material in the form of vortices. Each vortex appearing carries a flux quantum, $\phi = \frac{h}{2e}$ and consists of both a cylindrical core of a radius ξ, named as coherence length and a current circulating around the core out to a distance λ, called as penetration depth of the material [58]. The coherence length and penetration depth, from important parameters of the superconductivity, can hardly be determined. However, the ξ at the absolute zero temperature can be inferred from the upper critical magnetic field. The coherence length ξ0 at T=0 K is defined as,

$$\xi = \left[\frac{\emptyset_0}{2\pi H_{c2}(T)\mu_0}\right]^{\frac{1}{2}} \tag{5.4}$$

where $\emptyset_0 = 2{,}07 \times 10^{-5} Tm^2$. The ξ_0 values calculated from the equation (11) are listed in Table 5. Further, as reported in literature, we can calculate the penetration depth with the aid of the relation [60],

$$\kappa = {}^{\lambda}/_{\xi_0} \tag{5.5}$$

where the approximation value of κ (the Ginzburg–Landau parameter) is 2.6 A° [60].

Table 5 Irreversibility field, upper critical field, coherence length and penetration depth values of the samples

Samples	$\mu_0 H_{c2}(0)$	$\mu_0 H_{irr}(0)$	ξ_0(Å)	λ_0(Å)	κ
Sm0	98.1	14.1	18.33	48.35	2.64
Sm1	123.2	14.6	16.34	47.52	2.91
Sm2	174.2	17.2	13.76	43.78	3.18
Sm3	224.6	18.4	12.11	42.33	3.50
Sm4	315.6	18.7	10.22	41.99	4.11
Sm5	350.2	21.2	9.51	39.43	4.15
Sm6	90.3	13.5	19.12	49.41	2.59

5.3 XRD Measurements Analysis

X-ray diffraction (XRD) data were taken using a Rigaku D/Max-IIIC diffractometer with CuKα radiation in the range 2Θ = 3°- 60° with a scan speed of 3 °/min and a step increment of 0.02° at room temperature. The XRD measurements give some information about lattice parameters. In other words, these data provide to understand that phase purity and grains size by using XRD patterns. It is necessary to underline that the crystal structure of an unknown material can be found by using XRD patterns. Moreover, it is supplied to determine the orientation of a single crystalline or grain and evaluate the average spacings between layers or rows of atoms.

Table 6 XRD, J_c, bulk density (ρ) and porosity (P) values for the samples prepared

Samples	***a*** **(Å)**	***c*** **(Å)**	***Volume fraction (%)***		***Grain Size*** **(nm)**	***ρ (g/cm3)***	***P (%)***
			2223	***2212***			
Sm0	5.39	36.88	58	42	43.09	5.582	11.425
Sm1	5.35	37.02	63	37	46.44	5.786	8.188
Sm2	5.32	37.07	71	29	49.13	5.809	7.823
Sm3	5.31	37.11	77	23	51.52	5.822	7.617
Sm4	5.29	37.32	79	21	60.09	5.973	5.221
Sm5	5.28	37.41	83	17	71.13	5.987	4.998
Sm6	5.42	36.52	52	48	39.66	5.404	14.249

It can be inferred from the (00 l) planes diffraction with high intensity in XRD patterns in the Table 2 that the resistance in the path is mainly reflected in the information of ab-plane resistance, which is derived from the Bi-2223 grains with the plate-like structure. When the powders with different grain orientations are compressed into the pellets with an isostatic pressure, most of the grains with the plate-like structure tend to have c-axis orientation. The grain size, lattice parameters, porosity, volume fraction and density of samples were evaluated via XRD data as seen Table 2.

Texturing, porosity, crystal structure and phase compositions are characterized by XRD investigations using a Rigaku Multiflex+ XRD diffractometer with CuKα radiation (λ = 1.5418 Å) in the range 2θ = 3−60° at a scan speed of 3°/min and a step increment of 0.02° at the room temperature. The accuracy in the determination of the cell parameters (a and c) is found to be ±0.0001 Å. Moreover, the grain connectivity and surface morphology of the samples prepared in this work are identified using a Jeol scanning electron microscope (SEM) JEOL 6390-LV, operated at 20 kV, with a resolution power of 3 nm.

Transport properties of the grain boundaries in the $Bi_{2-x}Sr_{1.9}Ca_{2.1}Cu_{3.2}Sm_xO_y$ superconducting materials are characterized with the aid of the density measurements based on Archimedes water displacement method and the density of the pure BSCCO system is approximately used to be 6.302 g/cm^3 in the theoretical density calculations [61]. The density values obtained are displayed in Table 2. One can see from the table that the relative densities of the new systems change from 5.973 to 5.572 g/cm^3. The former (maximum) value belongs to the Sm4 sample whereas the minimum value is observed for the Sm6 sample. Moreover, the density of 5.582 g/cm^3 is obtained for the pure sample.

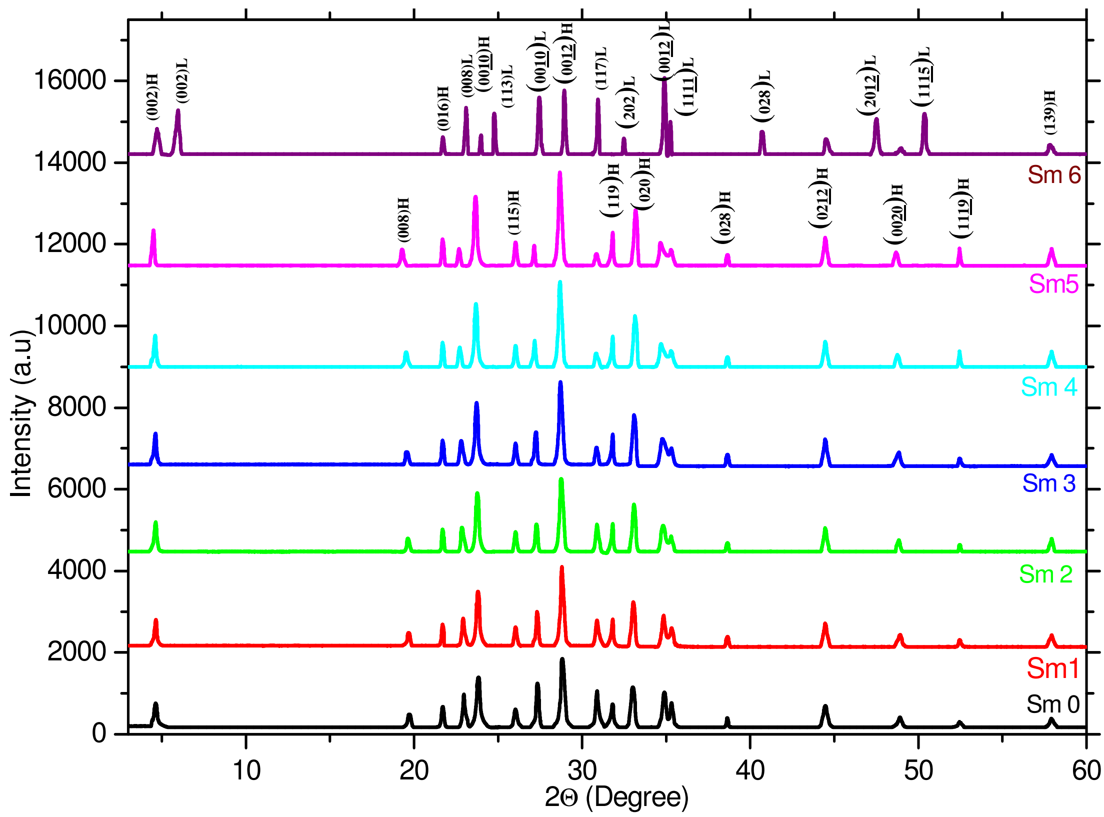

Fig. 5.5 XRD patterns for all the samples studied

In addition, the cell parameters *a* and *c* are computed by means of the least square method through *d* values and (*h k l*) planes for tetragonal unit cell structure. The *a* and *c* parameters calculated are tabulated in Table 2. As seen from the table, there is a systematic change for both parameters. Namely, a systematic contraction in the *a*-axis length is noted while a regular elongation in the *c*-axis length is observed with the increment of the Samarium substitution until the content level of x=0.07 beyond which the feature of both parameters completely converses: a monotonous expansion in the *a* and reduction of the *c* parameters, respectively. It means that the lattice parameter *a* is controlled by the Cu–O bond length in the Cu–O_2 (in-plane) planes which are responsible for the sizes in the basal planes corresponding to the Bi-2223 system [62-65].

5.4 SEM Measurements Analysis

The micrographs taken in the secondary electron image mode at 3000-X magnification by means of the Scanning Electron Microscopy (SEM) are used to explore the morphological features of the pure and Sm substitution with bulk superconducting materials studied in this work. The typical results obtained are depicted in Fig. 3. It is apparent from the figure that the microstructures of the samples are strongly dependent upon the level of Sm inclusions inserted in the Bi-2223 system. All the samples prepared exhibit a greatly dense surface with a fine connectivity between the grains. In particular, the surface of the Sm5 sample is much smoother and denser with the clear and flaky layers of large platelet-like structure (the basic characteristics of Bi-2223 phase formation) compared to other ones [66–68]. Additionally, the sample has more uniform surface appearance with larger grains, lower porosity, better texturing, crystallinity and connectivity between grains as shown in Fig. 3.

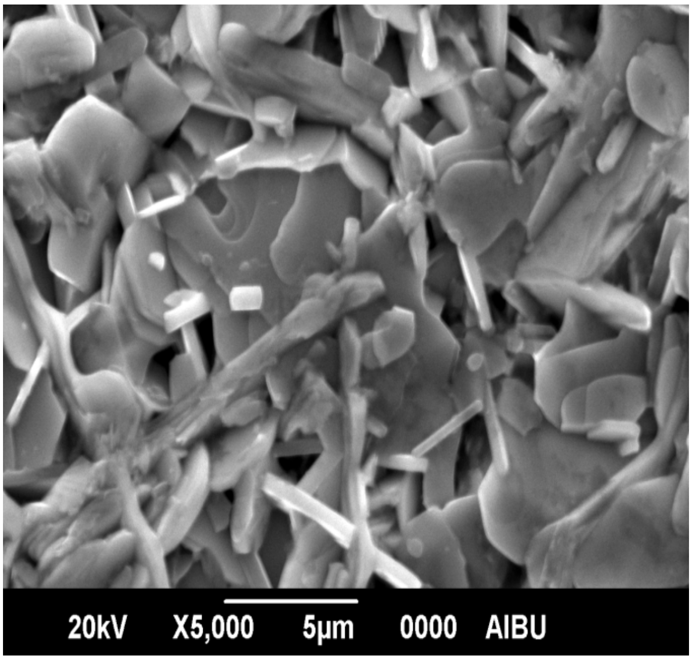

Fig. 5.6 SEM micrographs for the samples prepared

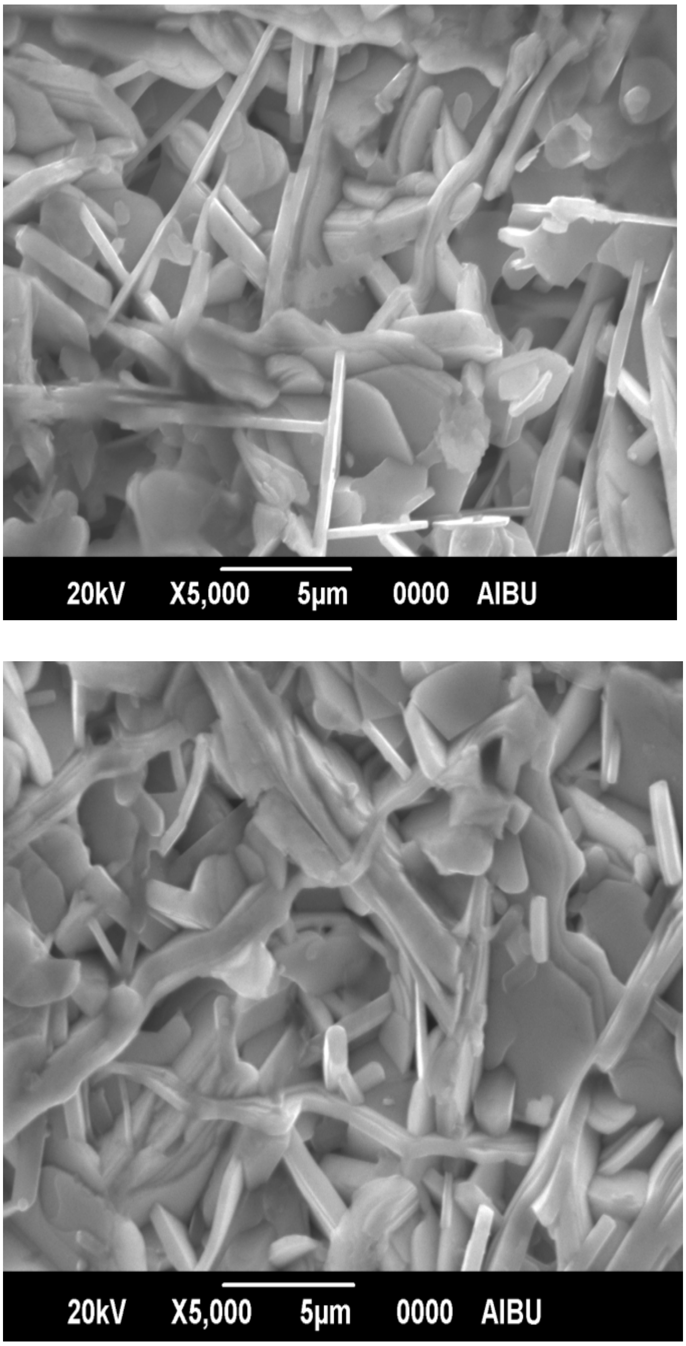

Fig. 5.6 SEM micrographs for the samples prepared (Continued).

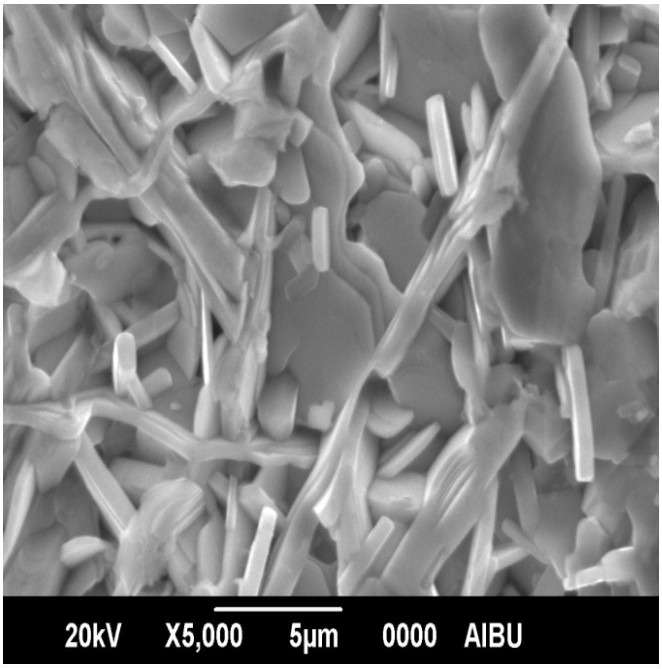

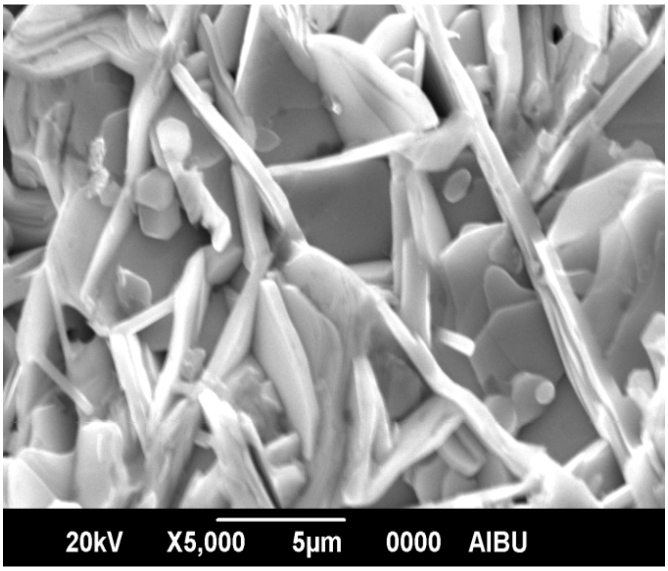

Fig. 5.6 SEM micrographs for the samples prepared (Continued).

5.5 Microhardness Measurements Analysis

Vickers microhardness measurements of the samples studied are carried out in air using digital microhardness tester (SHIMADZU HVM-2). The load in the range of 0.245N-2.940N is applied for all the trials during 10 seconds and the diagonals of indentation are measured with an accuracy of ±0.1μm. An average of five readings at different locations of the specimen surfaces is taken to obtain reasonable mean values for each load.

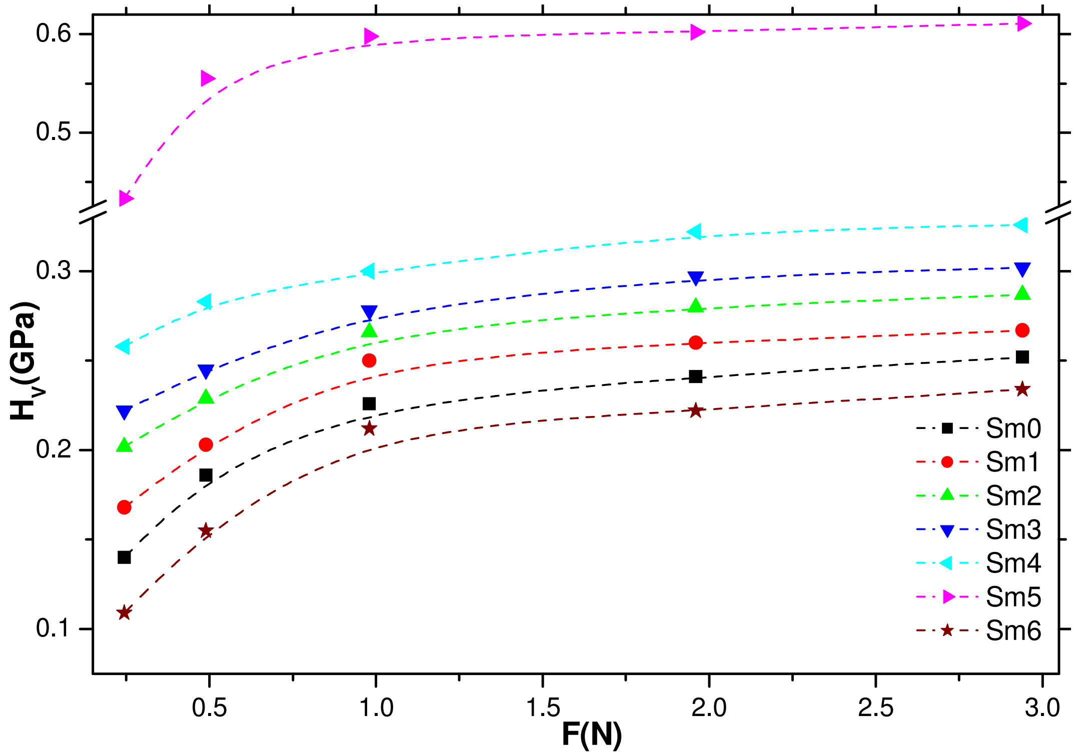

Fig. 5.7 Variation of load dependent microhardness H_v as a function of the various applied load F for RISE behaviors.

Table 7 The calculated load dependent H_v, E and Y for the samples produced

Samples	Hv (GPa)	E(GPa)	Y(Gpa)
Sm 0	0,14	11,47489	0,046667
	0,186	15,24521	0,062
	0,226	18,52375	0,075333
	0,241	19,7532	0,080333
	0,252	20,6548	0,084
Sm 1	0,168	13,76987	0,056
	0,203	16,63859	0,067667
	0,25	20,49088	0,083333
	0,26	21,31051	0,086667
	0,267	21,88425	0,089
Sm 2	0,212	17,37626	0,070667
	0,229	18,76964	0,076333
	0,269	22,04818	0,089667
	0,28	22,94978	0,093333
	0,287	23,52352	0,095667
Sm 3	0,222	18,1959	0,074
	0,245	20,08106	0,081667
	0,278	22,78585	0,092667
	0,297	24,34316	0,099
	0,302	24,75298	0,100667
Sm 4	0,266	21,80229	0,088667
	0,289	23,68745	0,096333
	0,3	24,58905	0,1
	0,322	26,39225	0,107333
	0,326	26,7201	0,108667
Sm 5	0,433	35,4902	0,144333
	0,555	45,48974	0,185
	0,598	49,01417	0,199333
	0,602	49,34203	0,200667
	0,611	50,0797	0,203667
Sm 6	0,109	8,934022	0,036333
	0,155	12,70434	0,051667
	0,212	17,37626	0,070667
	0,222	18,1959	0,074
	0,234	19,17946	0,078

CHAPTER 6

CONCLUSION

The aim of this study is to examine the change of the electrical, microstructural, mechanical and superconducting properties with the content level of the Sm substitution with Bi in Bi-2223 matrix with the aid of the dc resistivity, transport critical current density, X-Ray diffraction analysis, scanning electron microscopy, Vickers microhardness and density measurements. From the resistivity curves, the room temperature resistivity, onset and offset transition critical temperature and variation of transition temperature values of the samples are investigated; similarly, the critical current density measurements help us to determine the variation of the flux pinning centers and the boundary weak-links between the superconducting grains.

Additionally, the SEM investigations allow us to discuss the surface morphology, grain connectivity crystallinity, porosity, and grain size distribution of the samples. Furthermore, the texturing, phase purity, crystal structure, grain size and cell parameter are analyzed from the XRD patterns of the samples studied. All the results obtained confirm that there is a strong relationship between superconducting, microstructural and mechanical properties of the Sm substituted bulk Bi-2223 superconducting materials. It is evident from the XRD patterns that all samples have dominant peaks of the "2223" phase, together with only small peaks from the "2212" phase and others. Sample Sm 5 has the lowest level of second phases and the highest degree of the c-axis alignment in all samples, which is related to the highest J_{co} value. According to Bragg's Law, it is neccessary to underline that the angle is related with the properties of superconducting which becomes better during the angle decreases in XRD patterns.

Like the resistivity of the system, both the T_c^{onset} and T_c^{offset} values initially enhance with the Sm substitution until x=0.3 and after this point there is a dramatic decrease in these values, being favored by the variation of crystallinity, grain size and hole concentration state.

The greatest T_c^{onset} of 113.48K and T_c^{offset} of 109.82K are observed for the Sm 5 sample (substituted with x=0.1) whereas the Sm 6 sample (substituted with x=0.3) obtains the minimum values of 109.01K for the T_c^{onset} and 94.29K for the T_c^{onset} value. The ΔT_c value is found to be about 3.66K and 14.72K for the Sm 5 and Sm 6 sample, respectively, confirming that the excess Sm substituting is unfavourable for the velocity of the Bi-2223 phase formation.

According to the variable diffraction line intensities and lattice parameters *a* and *c* with regard to the content level, the substitution of Sm entering into the Bi-2223 crystal structure form the nanoparticles in the grain boundaries. These highly dispersed nanoparticles behaving as the nucleation (effective flux pinning) centers for vortices in the Bi-2223 material are tightly bound to the centers.

In a field tilted with respect to the CuO_2 planes, pancake vortices should be produced on the CuO_2 planes and be weakly pinned only by an extrinsic origin such as imperfections and precipitates, so that J decays significantly. The grain boundries resistivities decrease due to the variations of the critical temperature, also it causes a decrease of porosity. The grain boundry resistivity is associated with the weak links in second type of superconductors.

All samples indicated the metallic property which is explained by the interaction of electron and phonon. In other words, metallic properties can be explained by logarithmic change of the electrons in fermi level. The Pseduo transition is observed in the sample Sm 6 because the second phase (2212) was dominant in this sample. Moreover the residue resistivity ratio (RRR) shows how to have a good bond between the intergrains.

The Vickers microhardness measurements present that the samples exhibit the RISE feature as a consequence of the improvement of the grain connectivity (bond strength) between superconducting grains. The mechanical properties of superconductors are associated with J_c, T_c and H_v as proportionally. When the concentration of Samarium substitution rised, the increasing of H_v values are observed.

The very short superconducting coherence lengths of the oxide superconductors make their electrical and magnetic properties exceedingly sensitive to microstructural inhomogenety thus placing stringent requirements on the quality of grain boundaries.

Consequently, the concentration of Sm (x=0.1) behaves such as milestone in this experiment due to the fact that the results indicated the sample Sm 5 has the higgest both the critical temperature and the critical magnetic field.

REFERENCES

[1] Superconductivity Physics and Applications, Kristian Fossheim and Asle Sudbø, The Norwegian University of Science and Technology Trondheim, Norway.

[2] M. Yilmazlar, H.A. Cetinkara, M. Nursoy, O. Ozturk, C. Terzioglu, Thermal expansion and Vickers hardness measurements on $Bi_{1.6}Pb_{0.4}Sr_2Ca_{2-x}Sm_xCu_3O_y$ superconductors, Physica C 442 101–107, 2006.

[3] D. Yegen, A. Varilci, M. Yılmazlar, C. Terzioglu, I. Belenli, Magnetic properties of Sm-doped Bi-2223 superconductor studied by low field local Hall generator ac susceptibility, Physica C 466 5–10, 2007.

[4] C. Terzioglu, H. Aydin, O. Ozturk, E. Bekiroglu, I. Belenli, The influence of Gd addition on microstructure and transport properties of Bi-2223, Physica B 403 3354– 3359, 2008.

[5] I. Belenli, Ph.D. Thesis, 1993.

[6] H. K. Onnes, Superconductivity and Magnetism, Common Phys. Lab Unive Leiden, 119-120, 1911.

[7] J. R. Schrieffer, The Microscopic Theory of Superconductivity, Journal of Superconductivity, 4-5, 1911.

[8] W. Meissner, R.Ochsenfeld, Upper Critical Fields of High Tc Superconducting, 931-935, 1933.

[9] Selected by Science Educators, The History of Superconductors, www.superconductors.org, 2006.

[10] R. Hott, Materials Aspect of High Temperature Superconductors for Applications, 2003.

[11] J.G. Bednorz, and K. A. Müller, Possible HighTc Superconductivity in the Ba-La-Cu-O system, Z. Phys, 64 189-190, 1986.

[12] J.G. Bednorz, and K. A. Müller, The Discovery a Class of High Temperature Superconductors, Science, 237 1133-1139.

[13] High-Temperature Superconductors, Ajay Kumar Saxena.

[14] Introduction to Solid State Physics, C., Kittel, JohnWiley and Sons Inc, 1986.

[15] J. C. Gallop, Superconductivity, Science Technoloji, 20, 1990.

[16] N. W. Arhcraft, and N. D. Mermin, Solid State Physics, Holt Rinehart and Wiston, 1976.

[17] Superconductivity: The Meissner Effect, Persistent Currents and the Josephson Effects, MIT Department of Physics, February 8, 2011.

[18] Anonyms, Type-I Superconductors, Selected by Science Educators, www.superconductors.com, 2006a.

[19] Anonyms, Type-II Superconductors, Selected by Scince Educators, www.superconductors.com, 2006b.

[20] R. Clem, Melt texturing of BSCCO superconductor using an Infrared Lamp Image Furnace, 1998.

[21] Available in: http://hyperphysics.phy-astr.gsu.edu/hbase/solids/chrlen.html#c1.

[22] B. D. Josephson, Phys Lett. 1, 251, 1962.

[23] J.R. Christman, Fundementals of Solid State Physics, John Wiley & Sons,1988.

[24] Anonyms, High Temperature Superconductors, Wikipedia, The Free Encyclopedia, www.wikipedia.org, 2006.

[25] Anonyms, Superconductor Terminology, Selected by Science Educators, www.superconductors.com.

[26] A. Georgeta, Crystal Structures of Some High Temperature Superconductors, 2004.

[27] N. Ichinose, and K. Saito, Grain Orientation of the Bi-Sr-Ca-Cu-O System Ceramics by Hot-Forging and Their Superconducting Properties, Physica C, 190 177-179, 1991.

[28] S. N. Cassidy, L. F. Cohen, M. N. Cuthbert, S. Dou, and A. D. Caplin, Unusual form of the Temperature and Field Dependence of the Grain Boundary Weak-Link Dissapition in Ag Sheated BSCCO (2223) tapes.

[29] R. Clem, Melt texturing of BSCCO superconductor using an Infrared Lamp Image Furnace, 1998.

[30] Ö. Öztürk, Thesis of Master, Abant Izzet Baysal University, 2002.

[31] K. Kocabas, O. Ozkan, O. Bilgili, Y. Kadıoglu, H. Yılmaz, J. Supercond. Nov. Magn. 23, 1485–1492, 2010.

[32] D. Yazici, M. Erdem, B. Ozcelik, J. Supercond. Nov. Magn. 25, 293–297, 2012.

[33] M. Dogruer, Y. Zalaoglu, A. Varilci, C. Terzioglu, G. Yildirim, O. Ozturk, J. Supercond. Nov. Magn. 25, 961–968, 2012.

[34] O. Ozturk, E. Asikuzun, G. Yildirim, J. Mater. Sci: Mater. Electron, doi: 10.1007/s10854-012-0918-z, 2012.

[35] S.B. Guner, O. Gorur, S. Celik, M. Dogruer, G. Yildirim, A. Varilci, C. Terzioglu, J. Alloy. Compd. 540, 260–266, 2012.

[36] A. Ianculescu, M. Gartner, B. Despax, V. Bley, Th Lebey, R. Gavrila, M. Modreanu, Appl. Surf. Sci. 253, 344–348, 2006.

[37] D. Mangapathi Rao, T. Somaiah, V. Haribabu, Y.C. Venudhar, Cryst. Res. Technol. 28, 285–298, 1993.

[38] K. Kocabas, O. Ozkan, O. Bilgili, Y. Kadıoglu, H. Yılmaz, J. Supercond. Nov. Magn. 23, 1485–1492, 2010.

[39] H. Yamasaki, K. Endo, S. Kosaka, M.Umeda, S. Yoshida, K. Kajimura, Phys. Rev. Lett. 70, 3331,1993.

[40] J.T. Kucera, T.P. Orlando, G. Virshup, J.N. Eckstein, Phys. Rev. B 46, 11004, 1992.

[41] G. Yildirim, M. Dogruer, O. Ozturk, A. Varilci, C. Terzioglu, Y. Zalaoglu, J. Sup. Novel Mag., doi: 10.1007/s10948-011-1384-1, 2011.

[42] G. Yildirim, S. Bal, A. Varilci, J. Supercond. Nov. Magn., doi: 10.1007/s10948-012-1497-1, 2012.

[43] X. Yang, T.K. Chaki, Supercond. Sci. Technol. 6, 343–348, 1993.

[44] E. Yucel, C. Terzioglu, A. Varilci, A. Gencer, I. Belenli, Chinese J. Phys. 49 809–821, 2011.

[45] J.M. Rowell, Supercond. Sci. Technol. 16 R17–R27, 2003.

[46] C.J. Poole, H.A. Farach, R. Creswick, Superconductivity Academic Press, San Diego, pp. 320–321, 1995.

[47] R.R. Reddy, M. Murakami, S. Tanaka, P.V. Reddy, Physica C 257 137–142, 1996.

[48] J. Gong, J. Wu, Z. Guan, J. Eur. Ceram. Soc. 19 2625–2631, 1999.

[49] A.A. Elmustafa, D.S. Stone, J. Mech. Phys. Solid 51 357–381, 2003.

[50] C.B. Eom, M.K. Lee, J.H. Choi, L.J. Belenky, X. Song, L.D. Cooley, M.T. Naus, S. Patnaik, J. Jiang, M. Rikel, A. Polyanskii, A. Gurevich, X.Y. Cai, S.D. Bu, S.E. Babcock, E.E. Hellstrom, D.C. Larbalestier, N. Rogado, K.A. Regan, M.A. Hayward, T. He, J.S. Slusky, K. Inumaru, M.K. Haas, R.J. Cava, Nature 411, 558, 2001.

[51] Y. Iwasa, D.C. Larbalestier, M. Okada, R. Penco, M.D. Sumption, X.X. Xi, IEEE Trans. Appl. Supercond. 16, 1457, 2006.

[52] A. Yamamoto, J. Shimoyama, S. Ueda, Y. Katsura, I. Iwayama, S. Horii, K. Kishio, Appl. Phys. Lett. 86, 212502, 2005.

[53] M.D. Sumption, M. Bhatia, S.X. Dou, M. Rindfliesch, M. Tomsic, L. Arda, M. Ozdemir, Y. Hascicek, E.W. Collings, Supercond. Sci. Technol. 17, 1180, 2004.

[54] D.C. Larbalestier, L.D. Cooley, M.O. Rikel, A.A. Polyanskii, J. Jiang, S. Patnaik, X.Y. Cai, D.M. Feldmann, A. Gurevich, A.A. Squitieri, M.T. Naus, C.B. Eom, E.E. Hellstrom, R.J. Cava, K.A. Regan, N. Rogado, M.A. Hayward, T. He, J.S. Slusky, P. Khalifah, K. Inumaru, M. Haas, Nature 410, 186, 2001.

[55] J. Chen, V. Ferrando, P. Orgiani, A.V. Pogrebnyakov, R.H.T. Wilke, J.B. Betts, C.H. Mielke, J.M. Redwing, X.X. Xi, Q. Li, Phys. Rev. B 74, 174511, 2006.

[56] V. Braccini, L.D. Cooley, S. Patnaik, D.C. Larbalestier, P. Manfrinetti, A. Palenzona, A.S. Siri, Appl. Phys. Lett. 81, 4577, 2002.

[57] J.E.A. Gümbel, G. Fuchs, K. Nenkov, K.H. Müller, L. Schultz, Appl. Phys. Lett. 80, 2725, 2002.

[58] S. Gupta, R.S. Yadav, N.P. Lalla, G.D. Verma, B. Das, Integr. Ferroelectr. 116, 68, 2010.

[60] D.K. Finnemore, J.E. Ostenson, S.L. Bud'ko, G. Lapertot, P.C. Canfield, Phys. Rev. Lett. 86, 2420, 2001.

[61] X. Yang, T.K. Chaki, Supercond. Sci. Technol. 6 343–348, 1993.

[62] P.M. Sarun, S. Vinu, R. Shabna, A. Biju, U. Syamaprasad, J. Alloy. Compd. 472 13–17, 2009.

[63] R. Shabna, P.M. Sarun, S. Vinu, A. Biju, U. Syamaprasad, J. Alloy. Compd. 493 11–16, 2010.

[64] A. Biju, P.M. Sarun, R.P. Aloysius, U. Syamaprasad, J. Alloy. Compd. 454 46–51, 2008.

[65] C. Nguyen-van-huong, C. Hinnen, J.M. Siffre, J. Mater. Sci. 32 1725–1731, 1997.

[66] R.R. Reddy, M. Murakami, S. Tanaka, P.V. Reddy, Physica C 257 137–142, 1996.

[67] J. Gong, J. Wu, Z. Guan, J. Eur. Ceram. Soc. 19 2625–2631, 1999.

[68] A.A. Elmustafa, D.S. Stone, J. Mech. Phys. Solid 51 357–381, 2003.